

THE ATOMIC TO MOLECULAR TRANSITION IN GALAXIES. I: AN ANALYTIC APPROXIMATION FOR PHOTODISSOCIATION FRONTS IN FINITE CLOUDS

MARK R. KRUMHOLZ*

Department of Astrophysical Sciences, Princeton University, Peyton Hall, Princeton, NJ 08544 and Department of Astronomy & Astrophysics, University of California, Santa Cruz, Integrative Sciences Building, Santa Cruz, CA 95060

CHRISTOPHER F. MCKEE

Departments of Physics and Astronomy, University of California, Berkeley, Campbell Hall, Berkeley, CA 94720-7304

JASON TUMLINSON

Yale Center for Astronomy and Astrophysics, Yale University, PO Box 208121, New Haven, CT 06520 and Space Telescope Science Institute, 3700 San Martin Dr., Baltimore, MD 21218

Accepted to the Astrophysical Journal, August 8, 2008

ABSTRACT

In this series of papers we study the structure of the atomic to molecular transition in the giant atomic-molecular complexes that are the repositories of most molecular gas in galaxies, with the ultimate goal of attaining a better understanding of what determines galaxies' molecular content. Here we derive an approximate analytic solution for the structure of a photodissociation region (PDR) in a cloud of finite size that is bathed in an external dissociating radiation field. Our solution extends previous work, which with few exceptions has been restricted to a one-dimensional treatment of the radiation field. We show that our analytic results compare favorably to exact numerical calculations in the one-dimensional limit. However, our more general geometry provides a more realistic representation than a semi-infinite slab for atomic-molecular complexes exposed to the interstellar radiation field, particularly in environments such as low-metallicity dwarf galaxies where the curvature and finite size of the atomic envelope cannot be neglected. For clouds that are at least 20% molecular we obtain analytic expressions for the molecular fraction in terms of properties of the gas and radiation field that are accurate to tens of percent, while for clouds of lower molecular content we obtain upper limits. As a side benefit, our analysis helps clarify when self-shielding is the dominant process in H₂ formation, and under what circumstances shielding by dust makes a significant contribution.

Subject headings: ISM: clouds — ISM: molecules — molecular processes — radiative transfer

1. INTRODUCTION

In galaxies such as the Milky Way, where atomic and molecular phases of the interstellar medium coexist, molecular clouds represent the inner parts of atomic-molecular complexes (Elmegreen & Elmegreen 1987). The bulk of the volume of the interstellar medium is filled with far-ultraviolet (FUV) photons capable of dissociating hydrogen molecules, and this radiation field keeps the majority of the gas atomic. Gas that is predominantly molecular is found only in dense regions where a combination of shielding by dust grains and self-shielding by hydrogen molecules excludes the interstellar FUV field. These molecular regions are bounded by a photodissociation region (PDR) in which the gas is predominantly atomic (Hollenbach & Tielens 1999, and references therein).

To date most work on the structure of PDRs has been limited to one-dimensional geometries, including unidirectional or bidirectional beams of radiation impinging on semi-infinite slabs or purely radial radiation fields striking the surfaces of spheres (e.g. Federman et al. 1979; van Dishoeck & Black 1986;

Black & van Dishoeck 1987; Sternberg 1988; Elmegreen 1993; Draine & Bertoldi 1996; Hollenbach & Tielens 1999; Browning et al. 2003; Allen et al. 2004). For these one-dimensional problems the literature contains both detailed numerical solutions and analytic approximations for the problem of radiative transfer and H₂ formation-dissociation equilibrium. These approaches yield good results when the PDR is thin compared to the cloud as a whole, or for PDRs that are in close proximity to hot stars whose radiation and winds have compressed the PDR into a slab-like geometry. Many nearby well-studied PDRs, such as the Orion bar, fall into this latter category. However, the one-dimensional approximation is much less appropriate for giant clouds being dissociated by the combined starlight of many distinct stars and star clusters, particularly when the atomic region constitutes a significant fraction of the total cloud volume. The problem is especially severe in galaxies with low metallicities and interstellar pressures, where the predominantly molecular parts of cloud complexes generally constitute a small part of the total mass and volume (e.g. Blitz & Rosolowsky 2006). In this case one cannot neglect either the curvature of the PDR or the finite size of the molecular region, and a higher-dimensional approach is preferable. Previous work in one dimension is therefore of limited use for the problem on which we focus:

*Hubble Fellow

Electronic address: krumholz@ucolick.org

Electronic address: cmckee@astro.berkeley.edu

Electronic address: tumlinson@stsci.edu

determining the atomic and molecular content of galaxies on large scales, under the combined effects of all the sources of dissociating radiation in that galaxy.

Considerably less work has focused on higher-dimensional geometries, since these require a treatment of the angular dependence of the radiation field and its variation with position inside a cloud. As a result all treatments of two- or three-dimensional radiation fields to date are purely numerical. Neufeld & Spaans (1996) consider spherical clouds and Spaans & Neufeld (1997) allow arbitrary geometries, but their method applies only in translucent clouds, and involves an approximate numerical integration of the transfer equation. Similarly, Liszt & Lucas (2000) and Liszt (2002) present models for PDRs in spherical clouds involving angular integration over the radiation field in radial bins, coupled with a relaxation method to determine the H_2 abundance at each radius. Neither of these approaches yield a simple analytic estimate of the size of the PDR or the molecular region, nor do they provide any insight into the dimensionless numbers that can be used to characterize the problem of PDR structure. Such estimates, and the accompanying physical insights, would allow modeling of clouds over a wide range of galactic environments without the need for a complex and numerically costly radiative transfer calculation to cover each case.

Our goal in this work is to revisit the problem of determining the size of a PDR in a finite cloud embedded in a multi-dimensional radiation field, and to derive analytic approximations for the structure of a PDR that will yield gross yet observable quantities such as the total atomic hydrogen column around a molecular region and the fraction of a cloud's volume in the atomic and molecular phases. As part of this work we determine the important dimensionless numbers that characterize the problem, and we provide a rough classification of PDRs based on them. The model we develop is capable of spanning the range from galaxies where the gas in atomic-molecular complexes is predominantly molecular and a slab treatment is appropriate to dwarf galaxies where only a tiny fraction of the ISM resides in the molecular phase. In future work (Krumholz, McKee, & Tumlinson, in preparation), we provide a more detailed application of the results derived here to the problem of determining the atomic to molecular ratios in galaxies. Before moving on, we do note that our focus on an analytic solution with a multi-dimensional radiation field, characterized by a few dimensionless numbers, has a price: our approach to the chemical and thermal physics of PDRs is significantly simpler than much previous work. We do not account for factors such as the temperature-dependence of rate coefficients or H_2 dissociation by cosmic rays. Our work is therefore less suited to making detailed predictions of the structures of individual PDRs than it is to making predictions for galactic-scale trends in atomic and molecular content.

We approach the problem of finite clouds by idealizing to the case of a spherical cloud embedded in an isotropic radiation field, since this allows us to explore the effects of finite cloud size and curvature while at the same time keeping the problem simple enough to admit an approximate analytic solution. Our approach is as follows: in § 2 we state the formal problem and introduce some physical approximations that are independent of geometry. In

§ 3 we derive an approximate analytic solution to the one-dimensional semi-infinite slab case, which allows us to demonstrate the underlying physical principles of our approach. In this section we also compare to a grid of numerical solutions and show that our approach produces good agreement. Then in § 4 we extend our approach to handle the case of a spherical cloud embedded in an isotropic radiation field. Finally we summarize and draw conclusions in § 5.

2. THE FORMAL PROBLEM

Consider a region of hydrogen gas where the number density of hydrogen nuclei is n , mixed with dust which has a cross section $\sigma_{\text{d},\nu}$ per H nucleus to radiation of frequency ν . The hydrogen is a mix of atoms and molecules, with a fraction f_{HI} of the nuclei in the form of HI and a fraction $f_{\text{H}_2} = 1 - f_{\text{HI}}$ in the form of H_2 . We consider frequencies ν that fall within the Lyman-Werner (LW) band from $\nu_1 = c/1120 \text{ \AA}$ to $\nu_2 = c/912 \text{ \AA}$, such that photons of that frequency can be resonantly absorbed by hydrogen molecules.

The equation of radiative transfer for a beam of radiation in direction \hat{e} passing through this gas is

$$\hat{e} \cdot \nabla I_\nu = -n \left(\frac{1}{2} f_{\text{H}_2} \sigma_{\text{H}_2,\nu} + \sigma_{\text{d},\nu} \right) I_\nu, \quad (1)$$

where I_ν is the radiation intensity at frequency ν and $\sigma_{\text{H}_2,\nu}$ is the cross section for absorption of radiation at frequency ν by a molecule of hydrogen. The value of $\sigma_{\text{H}_2,\nu}$ may change with position as the fraction of H_2 molecules in different quantum states changes. The total fraction of the gas in the molecular phase is determined by the balance between the rate of H_2 formation and dissociation,

$$f_{\text{HI}} n^2 \mathcal{R} = \frac{f_{\text{H}_2}}{2} n \int d\Omega \int_{\nu_1}^{\nu_2} d\nu \frac{I_\nu}{h\nu} \sigma_{\text{H}_2,\nu} f_{\text{diss},\nu}. \quad (2)$$

where \mathcal{R} is the rate coefficient for formation of H_2 molecules on dust grain surfaces and $f_{\text{diss},\nu}$ is the fraction of absorptions at frequency ν that yield dissociation of the H_2 molecule rather than decay back to a bound state.

Note that we do not include a source term in the transfer equation (1), because although most FUV photons absorbed by H_2 molecules do decay through a vibrational ladder via photon emission, the photons released in this process do not fall into the LW band. Thus, the transfer equation we have written is only valid for frequencies in the LW band. We have also neglected scattering of FUV photons by dust grains. Since scattering is highly forward-peaked at FUV wavelengths (e.g. Roberge et al. 1981), this approximation is reasonable as long as we take $\sigma_{\text{d},\nu}$ to be the absorption cross section, not the total cross section. We have also omitted other H_2 dissociation mechanisms other than LW photons, such as cosmic ray collisions and chemical reactions. These are significant only in nearly fully molecular regions where there are no significant numbers of LW photons present.

Equations (1) and (2), together with the atomic and dust physics that specify $\sigma_{\text{H}_2,\nu}$ and $\sigma_{\text{d},\nu}$ and a boundary condition that specifies I_ν on all rays entering the surface of a cloud, fully determine I_ν and f_{H_2} at all positions.

We cannot solve them exactly, but we can obtain an approximation that exposes the basic physical outlines of the solution. We begin by making two standard approximations, following Draine & Bertoldi (1996), to simplify the atomic physics.

First, it is convenient to simplify the transfer equation (1) by dividing by $h\nu$ to transform from intensity to photon number, and then by integrating over frequency in the LW band. In so doing we can exploit the fact that for realistic dust $\sigma_{d,\nu}$ is nearly independent of frequency in the LW band (Draine & Bertoldi 1996) to replace $\sigma_{d,\nu}$ with a constant value σ_d . Doing so gives

$$\hat{e} \cdot \nabla I^* = -n\sigma_d I^* - \frac{1}{2} n f_{\text{H}_2} \int_{\nu_1}^{\nu_2} d\nu \sigma_{\text{H}_2,\nu} I_\nu^*, \quad (3)$$

where $I_\nu^* = I_\nu/(h\nu)$ is the photon number intensity, i.e. the number of photons per unit time per unit area per unit solid angle per unit frequency that cross a given surface, and $I^* = \int_{\nu_1}^{\nu_2} d\nu I_\nu^*$ is the photon number intensity integrated over the LW band.

Second, we note that $f_{\text{diss},\nu}$ varies only weakly when integrated over frequency and over position within a PDR. Draine & Bertoldi (1996) show that over the width of a PDR it stays roughly within the range 0.1 – 0.2. Its value in free space depends on the assumed radiation spectrum; Draine & Bertoldi (1996) find $f_{\text{diss}} = 0.12$ in free space for their fiducial choice, while Browning et al. (2003) suggest $f_{\text{diss}} = 0.11$ as a typical value. For simplicity we adopt a constant value $f_{\text{diss},\nu} = f_{\text{diss}} = 0.1$ and take this constant out of the integral, reducing the dissociation equation to

$$f_{\text{HI}} n^2 \mathcal{R} = \frac{f_{\text{H}_2} f_{\text{diss}}}{2} n \int d\Omega \int_{\nu_1}^{\nu_2} d\nu I_\nu^* \sigma_{\text{H}_2,\nu}. \quad (4)$$

It is convenient at this point to produce a combined transfer-dissociation equation from (3) and (4). If we integrate equation (3) over solid angle $d\Omega$, we obtain

$$\nabla \cdot \mathbf{F}^* = -n\sigma_d c E^* - \frac{1}{2} f_{\text{H}_2} n \int_{\nu_1}^{\nu_2} d\nu \sigma_{\text{H}_2,\nu} I_\nu^*, \quad (5)$$

where

$$E^* \equiv \frac{1}{c} \int d\Omega I^* \quad (6)$$

$$\mathbf{F}^* \equiv \int d\Omega \hat{e} I^* \quad (7)$$

are the photon number density and photon number flux integrated over the LW band, respectively. We can then use equation (4) to substitute for the last term, yielding the combined transfer-dissociation equation

$$\nabla \cdot \mathbf{F}^* = -n\sigma_d c E^* - \frac{f_{\text{HI}} n^2 \mathcal{R}}{f_{\text{diss}}}. \quad (8)$$

3. SOLUTION IN ONE DIMENSION

3.1. Analytic Solution

We start by giving an approximate analytic solution to this formal problem for unidirectional radiation impinging on a one-dimensional semi-infinite slab in order to illustrate the physical principles behind our approach. Consider a region of gas of density n filling the half-space

$z > 0$, subjected to a dissociating radiation field of photon number intensity $I^* = 4\pi J_0^* \delta(|\hat{e} - \hat{z}|)$ that fills the half-space $z < 0$, where J_0^* is the angle-averaged intensity in free space. The corresponding free-space photon number density is $E_0^* = 4\pi J_0^*/c$, and the magnitude of the free-space photon flux is $F_0^* = cE_0^*$. For simplicity we neglect the (relatively weak) temperature-dependence of \mathcal{R} .

Since the radiation intensity everywhere at all z remains proportional to $\delta(|\hat{e} - \hat{z}|)$, it immediately follows that

$$\mathbf{F}^* = F^* \hat{z} = cE^* \hat{z}, \quad (9)$$

at all points, and the combined transfer-dissociation equation reduces to

$$\frac{dF^*}{dz} = -n\sigma_d F^* - \frac{f_{\text{HI}} n^2 \mathcal{R}}{f_{\text{diss}}}, \quad (10)$$

subject to the boundary condition that $F^* = F_0^*$ at $z = 0$. Since numerical calculations show that the transition from predominantly atomic gas to predominantly molecular gas in a PDR generally occurs in thin band bounded by much larger regions where the gas is either predominantly atomic or predominantly molecular, we can obtain a good approximation to the exact solution by treating f_{HI} as having a constant value near unity over the bulk of the PDR, and then dropping to zero as a step function once the fully molecular surface is reached. For constant $f_{\text{HI}} = 1$, we can non-dimensionalize equation (10) to

$$\frac{d\mathcal{F}}{d\tau} = -\mathcal{F} - \frac{1}{\chi}, \quad (11)$$

where $\mathcal{F} = F^*/(F_0^*)$ is the fraction of the free-space flux remaining, $\tau = n\sigma_d z$ is the dust optical depth from the slab surface, and

$$\chi = \frac{f_{\text{diss}} \sigma_d c E_0^*}{n \mathcal{R}}. \quad (12)$$

Equation (11) has the exact solution

$$\mathcal{F}(\tau) = \frac{1}{\chi} \left[e^{-(\tau - \tau_{\text{HI}})} - 1 \right], \quad (13)$$

where

$$\tau_{\text{HI}} = \ln(1 + \chi) \quad (14)$$

is the depth at which the flux goes to zero, which we take to be the optical depth through the HI region. Of course in reality the flux should never go to zero exactly. That is does in our solution is an artifact of our choice to treat f_{HI} as constant. Nonetheless, since the transition from $f_{\text{HI}} \approx 1$ to $f_{\text{HI}} \approx 0$ is sharp, $z_{\text{H}_2} = \tau_{\text{HI}}/(n\sigma_d)$ should be a good approximation of the depth at which the gas becomes predominantly molecular.

The dimensionless parameter χ/f_{HI} is the ratio of the two terms on the right hand side of equation (10) with F^* set equal to its value $4\pi I_0^*$ at the slab edge. This makes its physical meaning clear: χ/f_{HI} represents the ratio of the absorption rate of LW photons by dust grains to the absorption rate by H_2 molecules for a parcel of gas exposed to the unattenuated free space radiation field. If the gas at the edge of free space is predominantly atomic, as is the case for example at the edge of an atomic-molecular complex, then $f_{\text{HI}} \approx 1$ and this ratio is

simply given by χ . For $\chi > 1$ absorptions by dust grains dominate, while for $\chi < 1$ absorptions by H_2 molecules dominate.

For a giant molecular cloud in the Milky Way and its outer atomic envelope, typical values of the number density, dust cross section, and H_2 formation rate coefficient are $n \sim 30 \text{ cm}^{-3}$, $\sigma_d \sim 10^{-21} \text{ cm}^2$ and $\mathcal{R} \sim 3 \times 10^{-17} \text{ cm}^3 \text{ s}^{-1}$ (Draine & Bertoldi 1996). Using the Draine (1978) functional form for the local FUV radiation energy density as a function of wavelength,

$$\lambda E_\lambda = 6.84 \times 10^{-14} \lambda_3^{-5} (31.016 \lambda_3^2 - 49.913 \lambda_3 + 19.897) \text{ erg cm}^{-3} \quad (15)$$

the free-space photon number density from 912 – 1120 Å is $E_0^* = 7.5 \times 10^{-4} \text{ cm}^{-3}$. For an H_2 molecule in the ground state, this corresponds to a free-space dissociation rate of $3.24 \times 10^{-11} \text{ s}^{-1}$. (In principle for a slab computation we should divide the observed value of E_0^* by two to account for the fact that one can only see half the sky at the surface of an opaque cloud, but we do not do so here because in § 4 we will account for this effect self-consistently.) Thus, for Milky Way conditions not near a local strong source of FUV, χ of order a few might be typical. Thus, in the Milky Way dust shielding is marginally significant in determining the structure of atomic-molecular complexes.

3.2. The Two-Zone Approximation

We can integrate the transfer-dissociation equation (8) directly in one dimension because, due to the constant angular distribution of the radiation, there is a trivial relationship between E^* and F^* . In multiple dimensions, however, there is no simple relationship between the two, because the angular distribution of the radiation intensity is not constant with position inside a cloud. To overcome this problem, we adopt what we call the *two-zone approximation*. When the photon number density E^* is large, the first term on the right hand side of equation (8), representing absorptions of photons by dust grains, is much larger than the second term, representing absorptions by H_2 molecules. This makes intuitive sense: in regions where there many dissociating photons present, the molecular fraction will be very low, so there will be few H_2 molecules available to absorb LW photons and most photons will be absorbed by dust. In regions where E^* is small, the number of molecules will increase, and for any appreciable number of molecules these will dominate the absorption rate.

In the two-zone approximation, we divide the cloud into a zone where dust absorption dominates and a zone where molecular absorption dominates. In the dust-dominated region we drop the molecular absorption term in the radiative transfer or transfer-dissociation equations (equations 3 or 8), and approximate the opacity as having a constant value $n\sigma_d$. In the zone where molecular absorptions dominate, we drop the dust absorption term in equation (8) and approximate the molecular absorption term by $\phi n^2 \mathcal{R} / f_{\text{diss}}$, where $\phi > 1$ is a constant of order unity, whose precise value we determine below, that we include to account for the fact that some LW photons will be absorbed by dust grains even in the molecular-dominated region. We define a boundary between these two zones by the condition that the dust and molecular

absorption terms be equal, which is satisfied when

$$\frac{E^*}{E_0^*} = \frac{\phi}{\chi} \equiv \frac{1}{\psi}, \quad (16)$$

where we have set $f_{\text{HI}} = 1$ because at the point of equality the molecular fraction is $\ll 1$, and for convenience we have defined the modified dust to molecular absorption ratio $\psi = \chi/\phi$. With this approximation, the one-dimensional non-dimensionalized transfer-dissociation equation becomes

$$\frac{d\mathcal{F}}{d\tau} = - \begin{cases} \mathcal{F}, & \mathcal{F} > 1/\psi \\ 1/\psi, & \mathcal{F} < 1/\psi \end{cases} \quad (17)$$

We shall see in § 4 how the two-zone approximation enables us to solve the problem in the spherical case. First, though, we examine the solution in the one-dimensional case. If $\psi < 1$, then $\mathcal{F} < 1/\psi$ is satisfied everywhere and equation (17) has the trivial solution

$$\mathcal{F} = \frac{\psi - \tau}{\psi}. \quad (18)$$

The flux goes to zero at a depth $\tau_{\text{HI}} = \psi$. If $\psi > 1$, the solution is

$$\mathcal{F} = \begin{cases} e^{-\tau}, & \tau < \tau_d \\ \psi^{-1}(\tau_{\text{HI}} - \tau)/(\tau_{\text{HI}} - \tau_d), & \tau > \tau_d \end{cases}, \quad (19)$$

with

$$\tau_d = \ln \psi \quad (20)$$

$$\tau_{\text{HI}} = 1 + \ln \psi. \quad (21)$$

Here τ_d represents the dust depth into the slab at which the absorption begins to be dominated by H_2 molecules, while τ_{HI} is the optical depth where we expect a transition from mostly atomic to mostly molecular gas. Combining the two cases, we have

$$\tau_{\text{HI}} = \begin{cases} \psi, & \psi < 1 \\ 1 + \ln \psi, & \psi > 1 \end{cases}. \quad (22)$$

We now turn to the question of determining the constant ϕ . Physically, we expect to have $\phi \rightarrow 1$ for $\chi \ll 1$, because in that case dust absorptions contribute negligibly throughout the cloud. For $\chi \gg 1$ we expect to have ϕ to asymptote to a value greater than unity, accounting for the contribution of dust to absorptions even in the molecular-dominated region. A comparison of the limiting behavior of the analytic solution (14) with the two-zone approximation (22) confirms this physical argument, and suggests that the appropriate limiting behavior is $\phi \rightarrow 1$ as $\chi \rightarrow 0$ and $\phi \rightarrow e$ as $\chi \rightarrow \infty$. We therefore adopt

$$\phi = \frac{2.5 + \chi e}{2.5 + \chi}, \quad (23)$$

which has the correct limiting behavior, and where the value 2.5 is chosen to optimize agreement between the two-zone approximation and the analytic solution in the intermediate χ region.

3.3. Comparison to Numerical Calculations

Before using the two-zone approximation to compute the case of a finite cloud with an isotropic radiation field,

we check its accuracy for the one-dimensional case by comparing with detailed numerical calculations using the Browning et al. (2003) H₂ formation and radiative transfer code. We refer readers to that paper for a full description of the physics included in this calculation, but a brief summary is that the code numerically integrates the frequency-dependent equation of radiative transfer for a unidirectional beam of radiation incident on an isothermal, constant-density slab of gas mixed with dust. The transfer equation is coupled to a statistical equilibrium calculation that determines the populations of HI atoms and a large number of rotational and vibrational levels of the H₂ molecule that are excited by LW band photons in each computational cell. The output of this calculation is the fraction of H nuclei in molecules as a function of depth within the cloud. The code we use here differs from that described in Browning et al. (2003) only in that the earlier version accounted for absorptions of LW photons by dust grains by modifying the photodissociation rate using the method of van Dishoeck & Black (1986), whereas the version we use here computes radiation attenuation by dust grains directly from the radiative transfer equation.

For the models we present here we use a density and temperature of $n = 5000 \text{ cm}^{-3}$ and $T = 90 \text{ K}$. These values are chosen purely for computational convenience, and have no significant impact on the results. The incident radiation field is a unidirectional beam of photons uniformly distributed in frequency over the wavelength range $912 - 1120 \text{ \AA}$. The frequency-dependent photon flux in this beam is F_ν^* , so $E_0^* = F_\nu^*(\nu_2 - \nu_1)/c$ and $J_0^* = F_\nu^*(\nu_2 - \nu_1)/(4\pi)$. We adopt a dust extinction curve following the functional form of Cardelli et al. (1989), scaled to give a dust cross section per H nucleus at 1000 \AA of $\sigma = \sigma_{\text{d,MW}}Z'$, where Z' is the metallicity relative to solar and we take $\sigma_{\text{d,MW}} = 6.0 \times 10^{-22} \text{ cm}^2$ or $2.0 \times 10^{-21} \text{ cm}^2$ to be two fiducial dust opacities for the Milky Way. These two values of $\sigma_{\text{d,MW}}$ correspond to the estimated attenuation cross sections at 1000 \AA estimated by Draine & Bertoldi (1996) for dense and diffuse clouds Milky Way, respectively. We adopt a rate coefficient for H₂ formation on grain surfaces of $\mathcal{R} = \mathcal{R}_{\text{MW}}Z'$ with $\mathcal{R}_{\text{MW}} = 3 \times 10^{-17} Z' \text{ cm}^{-3} \text{ s}^{-1}$ as our fiducial Milky Way value (Wolfire et al. 2008). We do our computations for a grid of models running from $F_\nu^* = 10^{-7} - 10^{-3} \text{ photons cm}^{-2} \text{ s}^{-1} \text{ Hz}^{-1}$ in steps of nine steps of 0.5 dex, from $Z' = 10^{-2} - 10^{0.5}$ in six steps of 0.5 dex, and for the two values of $\sigma_{\text{d,MW}}$ mentioned above. These values F_ν^* are significantly higher than are typical in the Milky Way, but are chosen so that, in conjunction with our choice of n , the ratio E_0^*/n that appears in χ is within the typical Milky Way range. With this parameterization

$$\chi = 0.75(\sigma_{\text{d,MW},-21}/\mathcal{R}_{\text{MW}})(E_0^*/n_2) \quad (24)$$

$$= 4.07\sigma_{\text{d,MW},-21}F_{\nu,-5}^* \quad (25)$$

where $\sigma_{\text{d,MW},-21} = \sigma_{\text{d,MW}}/10^{-21} \text{ cm}^2$ is the Milky Way 1000 \AA dust absorption opacity normalized to 10^{-21} cm^2 , $E_0^* = E_0^*/7.5 \times 10^{-4} \text{ cm}^{-3}$ is the free-space dissociating photon number density normalized to the Milky Way value, $n_2 = n/100 \text{ cm}^{-3}$ is the number density of hydrogen nuclei in units of 100 cm^{-3} , and $F_{\nu,-5}^* = F_\nu^*/10^{-5}$

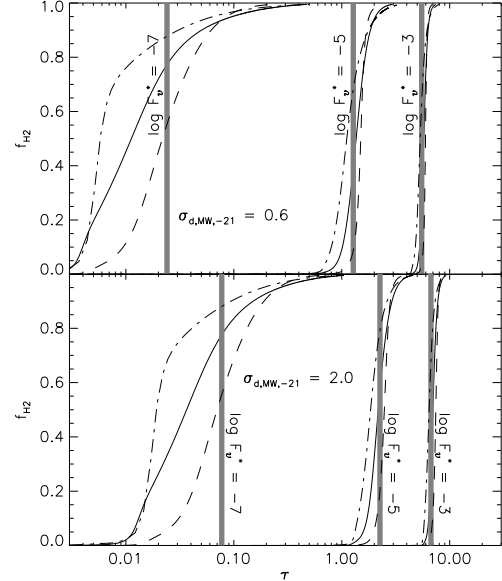


FIG. 1.— The plots show f_{H_2} versus dust optical depth $\tau = n\sigma_{\text{d}}z$ for our numerical radiative transfer calculations with $\log Z' = -1.5$ (dashed lines), $\log Z' = -0.5$ (solid lines), and $\log Z' = 0.5$ (dot-dashed lines). The gray vertical lines indicate the optical depth of the transition to fully molecular as calculated with the two-zone approximation, equation (22). Each cluster of three curves plus a vertical line indicating a prediction corresponds to a radiation flux $\log F_\nu^* = -7, -5, \text{ or } -3$, as indicated. The two panels are for the cases $\sigma_{\text{d,MW},-21} = 0.6$ and 2.0 , as indicated.

photons $\text{cm}^{-2} \text{ s}^{-1} \text{ Hz}^{-1}$. Thus the calculation covers a broad range of parameters from strongly dust-dominated to strongly molecular-dominated, thereby bracketing the real Milky Way value of $\chi \sim 1$. Note that χ is independent of Z' because for the parameterization we have chosen the Z' -dependences of σ_{d} and \mathcal{R} cancel. Since we predict that the dust optical depth through the PDR, $\tau_{\text{HI}} = n\sigma_{\text{d}}z_{\text{H}_2}$, depends only on χ , and χ in turn depends only on the ratio $\sigma_{\text{d}}/\mathcal{R}$, τ_{HI} should be independent of Z' . Since we use a range of $10^{2.5}$ in Z' , our numerical calculations represent a strong test of this prediction.

Figure 1 shows f_{H_2} versus depth within a cloud as computed numerically for a sample of our input parameters, overlaid with the corresponding locations of the atomic to molecular transition as calculated via the two-zone approximation. As the figure shows, the two-zone approximation does a very good job reproducing the location of this transition over an extremely broad range of parameters.

To quantify the quality of the approximation, we must define a fiducial measure for the depth of the H₂ region in the numerical calculations, since in these runs f_{HI} approaches but never reaches unity. The most reasonable measure is

$$N_{\text{HI}} = \int_0^\infty dz f_{\text{HI}} n, \quad (26)$$

the total HI column integrated through the cloud. Since the radiation field is attenuated exponentially or faster, and f_{HI} is proportional to radiation intensity in the region where $f_{\text{H}_2} \approx 1$, this integral is guaranteed to converge. In the limit where the transition from HI to H₂ is sharp it approaches the total gas column up to the

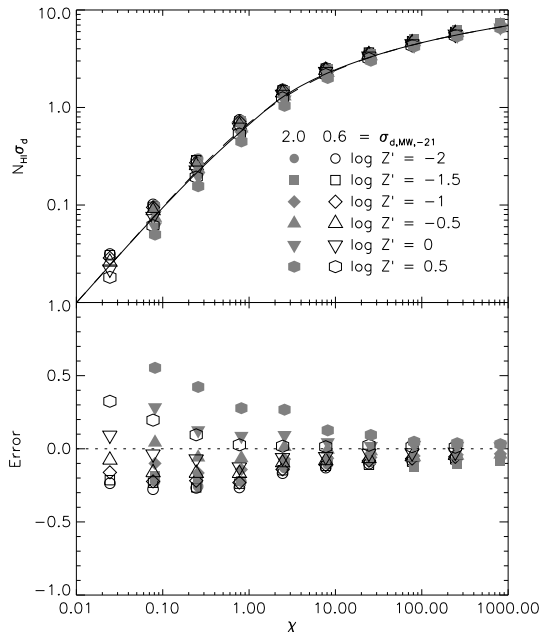


FIG. 2.— The upper panel shows the dust opacity $N_{\text{HI}}\sigma_{\text{d}}$ through the numerically-determined HI column (various symbols) as a function of χ . The values of Z' and $\sigma_{\text{d},\text{MW},-21}$ for each calculation are indicated by the plot symbol. This is compared to the optical depth τ_{HI} computed from the two-zone approximation (equation 22, thin solid line) and computed using the analytic solution (equation 14, thick dashed line). The lower panel shows the error in the two-zone approximation, defined as $\text{Error} = N_{\text{HI}}\sigma_{\text{d}}/\tau_{\text{HI}} - 1$; the dotted line indicates zero error.

transition point. In practice we cannot continue the numerical integration to $z = \infty$, so we truncate the integral at the value of z where $f_{\text{HI}} = 5 \times 10^{-3}$; using $f_{\text{HI}} = 10^{-2}$ instead changes the value by less than 8% for all our runs, and by less than 2% for all runs with $\chi > 0.1$, so our evaluation of the integral should be accurate to this level.

We plot the dust opacity through this hydrogen column, $N_{\text{HI}}\sigma_{\text{d}}$, and the corresponding value τ_{HI} predicted by the two-zone approximation, in Figure 2. As the figure shows, the two-zone approximation recovers the numerically-computed HI column to better than 50% accuracy over almost a five-decade range in χ . The error in the two-zone approximation is generally comparable to or smaller than the spread between models with different dust opacities but the same value of χ .

The error in our approximation is largest at small χ , and examination of Figure 1 suggests the reason why: by evaluating the equations with $f_{\text{HI}} = 1$ inside the PDR, we have assumed that the transition from atomic to molecular is sharp. This is true for $\chi \sim 1$ or greater, but begins to fail for $\chi \ll 1$. In our runs with $\chi \geq 1$, typically 95% of the gas is atomic in the region where $f_{\text{HI}} > 0.5$; and even at the depth where f_{HI} drops to 5×10^{-3} more than half the gas column above that point is atomic. This indicates a very sharp atomic-molecular transition, so our approximation that $f_{\text{HI}} = 1$ until the gas is almost entirely molecular is a good one. For $\chi \approx 0.01$, on the other hand, roughly 80% of the gas at $f_{\text{HI}} < 0.5$ is atomic, and HI contributes only 10% of the total gas column above $f_{\text{HI}} = 5 \times 10^{-3}$. The transition from atomic to molecular

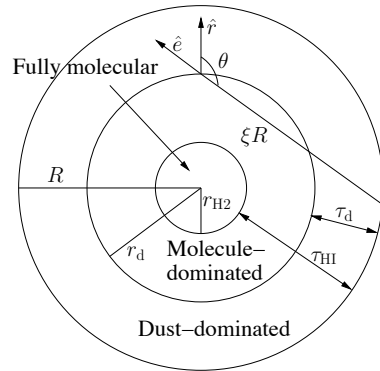


FIG. 3.— Illustration of the two-zone approximation in spherical geometry.

is therefore much more gradual, and our accuracy suffers as a result.

Nonetheless, we note that $\chi \ll 1$ does not appear to be physically realized in normal galactic environments. For Milky Way molecular clouds $\chi \sim 1$ or greater, and reducing χ to 0.01 would require some combination of reducing the ISRF and increasing the atomic gas density by a factor of 100. Such a combination of very high atomic ISM density and very low radiation field is generally not observed. We conclude that, for realistic physical parameters, and given that these parameters (such as σ_0 and \mathcal{R}) are themselves uncertain at the factor of a few level (e.g. Wolfire et al. 2008), the error in the two-zone approximation is unlikely to be the dominant one.

4. SOLUTION FOR SPHERICAL CLOUDS

We now extend the two-zone approximation to a spherical cloud of radius R embedded in a uniform, isotropic radiation field of angle-averaged intensity J_0^* . (Note that this radiation field has the same LW photon number density as the unidirectional radiation field considered in § 3, so it gives the same dissociation rate in free space.) Figure 3 illustrates the basic geometry of the problem and our approximation: we consider the dust-dominated region to run from radius $r = r_{\text{d}}$ to $r = R$, and the molecular self-shielding region to run from $r = r_{\text{H}_2}$ to $r = r_{\text{d}}$. For convenience we introduce the dimensionless position variables $x = r/R$ and $y = 1 - x$, and we define the dust optical depths from the surface to r_{d} and to r_{H_2} as τ_{d} and τ_{HI} , respectively.

In § 4.1 and § 4.2, we develop the basic equations that describe the two-zone approximation for clouds with and without dust opacity-dominated envelopes. We then explore three limiting cases of these equations. We consider the behavior at the boundary between the presence and absence of a dust-dominated zone in § 4.3, and we explore several interesting limits in § 4.4. We then give a numerical solution and an analytic approximation to it in § 4.5. In § 4.6 we compare our solution for a finite cloud to the standard slab approximation, to determine when the slab approximation is valid and when it fails. In § 4.7, we address the level of uncertainty introduced by the approximations we make in the spherical case. Finally, in § 4.8 we present some example calculations using our analytic approximation.

4.1. Clouds with Dust-Dominated Zones

First consider the case where ψ is large enough so that there is a dust-dominated zone in the outer part of the cloud where molecular self-shielding is negligible, i.e. $r_d < R$. The transfer equation in this region becomes

$$\hat{e} \cdot \nabla I^* = -n\sigma_d I^*, \quad (27)$$

which for rays originating at the cloud surface and staying entirely within the dust-dominated region has the trivial solution

$$I^*(x, \mu) = \exp(-\tau_R \xi) J_0^*, \quad (28)$$

where $\tau_R = n\sigma_d R$ is the center-to-edge dust optical depth of the cloud,

$$\xi = \left(\sqrt{1 - x^2 + x^2 \mu^2} - x\mu \right), \quad (29)$$

is the distance, normalized to the cloud radius, from radius r to the cloud surface on a ray that makes an angle θ relative to the radial vector (see Figure 3), and $\mu = \cos \theta = -\hat{e} \cdot \hat{r}$. This solution applies for $\mu > 0$. On the other hand, if $\mu < \mu_{\text{H}_2}$,

$$\mu_{\text{H}_2} \equiv -\sqrt{1 - \left(\frac{x_{\text{H}_2}}{x_d} \right)^2}, \quad (30)$$

then the ray passes through a part of the cloud that is fully molecular. Since the fully molecular region will be extremely opaque, to good approximation along these rays $I^*(x, \mu) = 0$. Finally, rays for which $0 > \mu > \mu_{\text{H}_2}$ pass through the region where the opacity is dominated by molecules rather than dust, but where the gas is not yet fully molecular. Again, we use the approximation that the transition from a low molecular fraction to fully molecular is sharp, so that over most of this region the molecular fraction is not vastly larger than it is at the region's edge. This is consistent with numerical solutions of the problem (e.g. Figure 1), which show that the atomic fraction f_{HI} is nearly constant through the bulk of the PDR, and rises from its free space value to unity over a small region. This means that the opacity is not much greater than its value of $n\sigma_d$ at the outer edge of the molecule-dominated region. We therefore approximate that the optical depth along these rays is the same as for those in the dust-dominated region, $\tau_R \xi$. This approximation is perhaps the least certain part of our calculation, and we quantify the level of uncertainty that it produces in § 4.7. Combining these three regions, we have an approximate intensity

$$I^*(x, \mu) = \begin{cases} \exp(-\tau_R \xi) J_0^*, & \mu > \mu_{\text{H}_2} \\ 0, & \mu < \mu_{\text{H}_2} \end{cases}. \quad (31)$$

The location of x_d , the crossover point from dust- to molecule-dominated absorption, is defined by the condition that $E^*/E_0^* = 1/\psi$ (equation 16). For convenience we define the function η_0 by

$$\frac{E^*(x_d)}{E_0^*} = \eta_0(x_d, x_{\text{H}_2}; \tau_R) = \frac{1}{2} \int_{\mu_{\text{H}_2}}^1 d\mu \exp(-\tau_R \xi_d), \quad (32)$$

where $\xi_d = \xi(x_d)$. We show that η_0 can be evaluated in terms of exponential integrals in Appendix A. The first

equation for the two-zone approximation is therefore

$$\eta_0(x_d, x_{\text{H}_2}; \tau_R) = \frac{1}{\psi}. \quad (33)$$

Inside x_d , we drop the dust opacity term, so that the combined transfer-dissociation equation (8) becomes

$$\frac{1}{r^2} \frac{d}{dr} (r^2 F^*) = \frac{\phi n^2 \mathcal{R}}{f_{\text{diss}}}, \quad (34)$$

where we have again assumed that $f_{\text{HI}} \approx 1$ outside the fully molecular region, and for convenience we have inverted the sign by defining $\mathbf{F}^* = -F^* \hat{r}$. The solution is

$$F^* = \frac{\tau_R}{3\psi} x \left[1 - \left(\frac{x_{\text{H}_2}}{x} \right)^3 \right] F_0^*, \quad (35)$$

where we have chosen the constant of integration by requiring that $F^* = 0$ at $x = x_{\text{H}_2}$. To determine x_{H_2} from the boundary conditions, however, we must determine the flux at some other location. Thus we evaluate the flux F^* at x_d by integrating the intensity over solid angle using equation (31). For convenience we define the function η_1 by

$$\frac{F^*(x_d)}{F_0^*} = \eta_1(x_d, x_{\text{H}_2}; \tau_R) = \frac{1}{2} \int_{\mu_{\text{H}_2}}^1 d\mu \mu \exp(-\tau_R \xi_d). \quad (36)$$

As with η_0 , in Appendix A we evaluate η_1 in terms of exponential integrals. Combining (36) with (35) gives an implicit equation for x_{H_2} :

$$\eta_1(x_d, x_{\text{H}_2}; \tau_R) = \frac{\tau_R x_d}{3\psi} \left[1 - \left(\frac{x_{\text{H}_2}}{x_d} \right)^3 \right]. \quad (37)$$

Together, equations (33) and (37) constitute two equations in the two unknowns x_d and x_{H_2} , and thus fully determine the location of the transition from predominantly atomic to predominantly molecular in the two-zone approximation.

4.2. Clouds without Dust-Dominated Zones

Now consider the case where ψ is small enough so that there is only one zone, because even gas at the edge of the cloud is sufficiently molecular for absorptions by molecules to outnumber those by dust grains. In this case equation (35) applies throughout the cloud, so we must fix x_{H_2} directly from the boundary conditions. To do so we need to know the flux $F^*(1)$ at the cloud surface. This is not simply $F_0^* = cE_0^*$ as in the case of a unidirectional radiation field; in free space for an isotropic radiation field F^* vanishes, and $F^*(1)$ is non-zero only because rays passing through the cloud do not carry the same intensity as rays that do not pass through it, preventing the integral over angle from vanishing. Thus for a sufficiently transparent cloud, $F^*(1)$ approaches zero, its value in free space. Conversely, at the surface of a cloud that is opaque and extremely large, $F^*(1) = F_0^*/4$. The factor of 1/4 relative to the unidirectional case arises because half the solid angle is blocked by an opaque object (providing one factor of 1/2), and because in the part of the sky that is not blocked the radiation is isotropic, and one must average over all the directions in which photons are traveling to find the fraction of that

motion in the $-\hat{r}$ direction (providing another factor of $1/2$).

The problem of determining the intensity is exactly the same as in § 4.1. At the surface of the cloud rays at angles $\mu > 0$ do not pass through the cloud and therefore contribute the unattenuated free space intensity I_0^* . Those with $\mu < \mu_{\text{H}_2} = -(1 - x_{\text{H}_2}^2)^{1/2}$ pass through the fully molecular region and therefore contribute zero intensity. For rays at angles $\mu_{\text{H}_2} < \mu < 0$, we make the same approximation as in § 4.1, that the molecular absorption rate per unit distance that a photon travels is roughly constant until one approaches the sharp transition from atomic to molecular. Thus the molecular opacity-dominated part of the PDR has a constant effective opacity, which we can determine by computing its value at the cloud surface. For convenience we characterize this opacity via an effective cross-section per H nucleus σ_e . By examining the transfer-dissociation equation (8), it is clear that for $f_{\text{HI}} \approx 1$ this opacity is

$$\sigma_e = \frac{\phi n \mathcal{R}}{f_{\text{diss}} c E^*(1)}. \quad (38)$$

With this approximation the transfer equation through the region outside where the gas becomes fully molecular is simply equation (27) with σ_d replaced by σ_e , and the solution for the intensity along each ray is given by equation (31) with τ_{R} replaced by $\tau_{\text{eR}} = (\sigma_e/\sigma_d)\tau_{\text{R}}$. The photon number density and flux at the cloud surface are therefore given by

$$\frac{E^*(1)}{E_0^*} = \eta_0(1, x_{\text{H}_2}; \tau_{\text{eR}}) \quad (39)$$

$$\frac{F^*(1)}{F_0^*} = \eta_1(1, x_{\text{H}_2}; \tau_{\text{eR}}). \quad (40)$$

With these arguments, evaluating equations (A11) and (A12) shows that η_0 and η_1 reduce to

$$\eta_0(1, x_{\text{H}_2}; \tau_{\text{eR}}) = \frac{1 - e^{2\mu_{\text{H}_2} \tau_{\text{eR}}}}{4\tau_{\text{eR}}} + \frac{1}{2} \quad (41)$$

$$\eta_1(1, x_{\text{H}_2}; \tau_{\text{eR}}) = \frac{(1 - 2\mu_{\text{H}_2} \tau_{\text{eR}})e^{2\mu_{\text{H}_2} \tau_{\text{eR}}} - 1}{8\tau_{\text{eR}}^2} + \frac{1}{4}. \quad (42)$$

Using these values of $E^*(1)$ and $F^*(1)$ in equations (38) and (35), we find

$$\frac{1 - e^{2\mu_{\text{H}_2} \tau_{\text{eR}}}}{4\tau_{\text{eR}}} + \frac{1}{2} = \frac{\tau_{\text{R}}}{\psi \tau_{\text{eR}}} \quad (43)$$

$$\frac{(1 - 2\mu_{\text{H}_2} \tau_{\text{eR}})e^{2\mu_{\text{H}_2} \tau_{\text{eR}}} - 1}{8\tau_{\text{eR}}^2} + \frac{1}{4} = \frac{\tau_{\text{R}}}{3\psi} (1 - x_{\text{H}_2}^3). \quad (44)$$

We therefore again have two equations in two unknowns, with the unknowns in this case being τ_{eR} and x_{H_2} . Note that in this case μ_{H_2} can be isolated in the first equation, to give

$$\mu_{\text{H}_2} = \frac{1}{2\tau_{\text{eR}}} \ln \left(1 + 2\tau_{\text{eR}} - \frac{4\tau_{\text{R}}}{\psi} \right). \quad (45)$$

Together with the relation between μ_{H_2} and x_{H_2} (equation 30), this reduces the problem to a single non-linear equation, which is convenient for numerical solution.

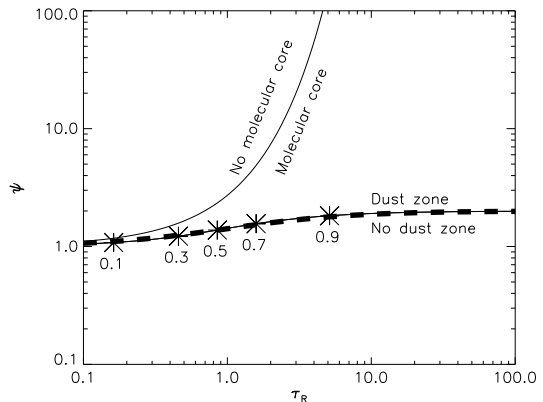


FIG. 4.— The thin black curves show the boundaries in the (τ_{R}, ψ) -plane at which $x_d = 1$, $\tau_{\text{eR}} = \tau_{\text{R}}$, and at which $x_{\text{H}_2} = 0$, as indicated by the text accompanying each curve. The thick dashed curve shows our approximation to the $x_d = 1$ curve, equation (47). The asterisks along the curve for $x_d = 1$ mark the points at which $x_{\text{H}_2} = 0.1, 0.3, 0.5, 0.7,$ and 0.9 , as indicated.

However, the two-equation form is more convenient for an analytic approach.

At this point it is worth making a few remarks about the behavior of equations (43) and (44). First, equation (43) implies that $\tau_{\text{R}}/(\psi \tau_{\text{eR}}) > 1/2$, so the argument of the logarithm in equation (45) is always less than unity and μ_{H_2} is negative. Second, in all of these equations τ_{R} and ψ appear only through the combination τ_{R}/ψ , so values of x_{H_2} and τ_{eR} must be constant on lines of constant τ_{R}/ψ . Finally, note that in § 4.5 we give an approximate analytic solution to equations (43) and (44).

4.3. The Dust-Dominated Zone Boundary

We first identify the boundary between the presence and absence of a dust-dominated region. In the case of a perfectly beamed radiation field impinging on a semi-infinite planar slab, which we treated in § 3, this is $\psi = 1$. The result is more complex in the case of an isotropic radiation field and a cloud of finite size. The boundary between the two cases is defined by the condition that $x_d = 1$ or $\tau_{\text{eR}} = \tau_{\text{R}}$, i.e. that the cross-over between dust-dominated and molecular-dominated absorptions occur at the cloud surface, or equivalently that the dust and molecular effective opacities at the cloud surface are equal. It is immediately obvious that equations (33) and (37) become identical to equations (43) and (44) in this limit. If we set $\tau_{\text{eR}} = \tau_{\text{R}}$, then equations (45) and (44) define a curve in the (τ_{R}, ψ) -plane that corresponds to the point where dust-dominated layer disappears. Above the curve the radiation field is strong enough so that the outer part of the cloud is dust opacity-dominated, while below it molecular opacity dominates throughout. Along the bounding curve,

$$x_{\text{H}_2} = \sqrt{1 - \frac{1}{4\tau_{\text{R}}^2} \left[\ln \left(1 + 2\tau_{\text{R}} - \frac{4\tau_{\text{R}}}{\psi} \right) \right]^2}. \quad (46)$$

We show the curve at which the dust-dominated layer vanishes, and the value of x_{H_2} along the curve, in Figure 4.

That along this curve $\psi \rightarrow 1$ for $\tau_{\text{R}} \ll 1$ and $\psi \rightarrow 2$ for $\tau_{\text{R}} \gg 1$ makes intuitive sense. If $\tau_{\text{R}} \ll 1$, the dust optical depth through the cloud is tiny and so the radiation field

has its unattenuated, free-space value regardless of position in the cloud. Thus the condition that dust shielding and molecular shielding contribute equally at the cloud surface ($x_d = 1$) can only be fulfilled if they are equal or nearly so in free space, which is simply a requirement that $\psi = 1$. Similarly, if $\tau_R \gg 1$ then the cloud is effectively a semi-infinite slab whose curvature is negligible. In this case the radiation field at the cloud surface only contains contributions from rays with $\mu > 0$, i.e. those that never pass through the cloud; rays with $\mu < 0$ are infinitely attenuated. Thus, the radiation field has exactly half its free-space value, the molecular fraction has double its free-space value, and the condition that dust shielding and molecular shielding are equal reduces to the requirement that $\psi = 2$.

These considerations suggest that a function that interpolates between these two limiting behaviors is likely to produce a good approximation. Numerical experimentation shows that the curve

$$\psi \approx \frac{1.4 + 2\tau_R}{1.4 + \tau_R} \quad (47)$$

reproduces the true value of ψ along the curve $x_d = 1$, $\tau_{eR} = \tau_R$ to better than 3% for all τ_R . We show this approximate solution with the thick dashed curve in Figure 4.

4.4. Limiting Cases

We can better understand the behavior of PDRs in finite clouds by exploring several limiting cases of our equations, corresponding to clouds that are very large or very small, and to radiation fields that are very strong or very weak.

Case 1: Strong Radiation Fields. The first limit we consider is one in which the radiation field is so strong that there is no fully molecular core, so $x_{H_2} = 0$. It is easy to verify that if there is no dust-dominated region, so equations (43) and (44) apply, then there are no finite values of ψ and τ_R such that $x_{H_2} = 0$. (However, see § 4.7, where we show that this behavior is probably not physical.) On the other hand, if there is a dust-dominated region, equations (33) and (37) apply and $x_{H_2} = 0$ can be reached at finite ψ and τ_R . This becomes clear if we note that $x_{H_2} = 0$ implies $\mu_{H_2} = -1$ (following equation 30), and equation (37) then admits the solution $x_d = \eta_1(x_d, 0; \tau_R) = 0$. Since $x_d = 0$, it immediately follows that $\xi_d = 1$ and $\eta_0(0, 0; \tau_R) = e^{-\tau_R}$. Equation (33) then gives $\psi = e^{\tau_R}$. The physical meaning of this solution is that $\psi = e^{\tau_R}$ is the critical curve along which $x_{H_2} = x_d = 0$; at this value of ψ or larger the radiation field is too intense for a fully molecular core to exist. We plot the critical curve in Figure 4. In Appendix B we solve equations (33) and (37) perturbatively in the vicinity of the critical curve, and show that near the strong radiation boundary the solution is

$$x_d = \left[\frac{6}{\tau_R(\tau_R + 2)} \left(\frac{e^{\tau_R}}{\psi} - 1 \right) \right]^{1/2} \quad (48)$$

$$x_{H_2} = \left[\frac{1536}{25\tau_R(\tau_R + 2)^3} \right]^{1/4} \left(\frac{e^{\tau_R}}{\psi} - 1 \right)^{5/4}. \quad (49)$$

This solution obviously only applies for $e^{\tau_R} \geq \psi$.

Case 2: Small Clouds. Before analyzing this case, we warn that in § 4.7 we show that our solution in this case should be regarded as giving an upper limit on the molecular fraction rather than a direct estimate. However it is still useful to consider this case, both in order to derive upper limits and to provide expressions that can be incorporated into approximations in parts of parameter space where our method does provide estimates rather than upper limits. We have shown that for $\psi > 1$, there is a finite value of τ_R at which the fully molecular core vanishes, and conversely that if $\psi < 1$ there is no finite τ_R for which $x_{H_2} = 0$. However, one can easily verify that when there is no dust-dominated zone ($\psi < 1$) and equations (43) and (44) apply, $x_{H_2} \rightarrow 0$ as $\tau_R \rightarrow 0$. Physically, this corresponds to the case of a cloud that is so small that its dust is optically thin to LW photons. In Appendix C we show that in this limit the solution may be approximated by

$$\tau_{eR} = \frac{\tau_R}{\psi} + \frac{\tau_R^2}{2\psi^2} + \frac{\tau_R^3}{4\psi^3} + \frac{7\tau_R^4}{60\psi^4} \quad (50)$$

$$x_{H_2} = \frac{\tau_R}{\sqrt{3}\psi} + \frac{2\sqrt{3}\tau_R^2}{5\psi^2}. \quad (51)$$

Note that by definition $\tau_{eR}/\tau_R = [E_0^*/E^*(1)]/\psi$, so equation (50) is effectively a series expansion for the photon number density at the cloud surface: $E^*(1) = E_0^*[1 - \tau_R^2/(2\psi) + \dots]$. Thus the leading-order approximation reduces to the statement that a small cloud blocks no radiation in any direction, so $E^*(1) = E_0^*$, the unattenuated value. The next-order correction accounts for the small fraction of photons that are blocked at the cloud surface.

Case 3: Large Clouds. Our final limiting case is that of a cloud so large that the transition from atomic to molecular gas occurs in a thin layer at the cloud surface, so that the cloud's curvature is negligible. Before proceeding we note that this case is *not* the same as the case of a one-dimensional slab subject to a unidirectional beam of radiation that we analyzed in § 3. The difference is that here the radiation field is isotropic, so it has an angular dependence that can vary with depth within the cloud. For this reason the large cloud limit with an isotropic radiation field is a two-dimensional problem even if the cloud is a semi-infinite slab. To analyze this case we perform a series expansion around the limit $\tau_R \rightarrow \infty$, but with $y_{H_2}\tau_R$ finite, so that there is a finite optical depth to the molecular region. If $\psi > 2$ then a dust-dominated zone exists, and we solve this problem by starting from equations (A11) and (A12) and series expanding η_0 and η_1 to first order in τ_R^{-1} . Doing so gives

$$\eta_0(x_d, x_{H_2}; \tau_R) = \frac{E_2(\tau_d)}{2} + \frac{e^{-\tau_d} + \tau_d E_2(\tau_d)}{4\tau_R} \quad (52)$$

$$\eta_1(x_d, x_{H_2}; \tau_R) = \frac{E_3(\tau_d)}{2} + \frac{\tau_d E_3(\tau_d)}{2\tau_R}, \quad (53)$$

where $\tau_d = y_d\tau_R$. Equation (33) therefore becomes

$$\frac{1}{\psi} = \frac{E_2(\tau_d)}{2} + \frac{e^{-\tau_d} + \tau_d E_2(\tau_d)}{4\tau_R} \quad (54)$$

to first order in τ_R^{-1} , which is straightforward to solve numerically to determine τ_d for a given ψ and τ_R . Alter-

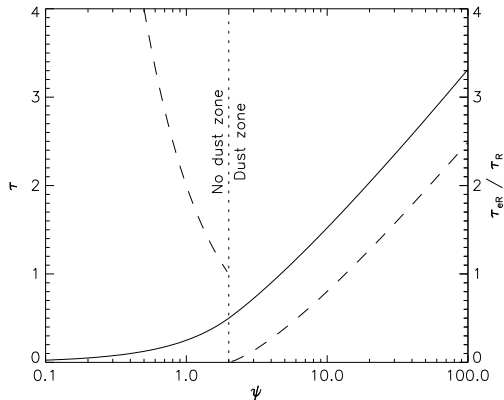


FIG. 5.— The plot shows the solution in the large cloud limit. The curves shown are the dust optical depth to the fully molecular region $\tau_{\text{HI}} = \tau_{\text{R}}(1 - x_{\text{H}_2})$ (solid curve), the dust optical depth to the point of dust-molecular absorption equality $\tau_{\text{d}} = \tau_{\text{R}}(1 - x_{\text{d}})$ (dashed curve to the right of $\psi = 2$), and the ratio of the effective molecular opacity to the dust opacity $\tau_{\text{eR}}/\tau_{\text{R}}$ (dashed curve to the left of $\psi = 2$). The dotted vertical line at $\psi = 2$ indicates the boundary between the presence and absence of a dust-dominated zone in the weak radiation limit.

nately, one may obtain a purely analytic expression by dropping the $1/\tau_{\text{R}}$ correction term. In this case the equation becomes $E_2(\tau_{\text{d}}) = 2/\psi$, which has the approximate solution

$$\tau_{\text{d}} \approx 0.83 \ln(0.2\psi + 0.6); \quad (55)$$

this expression is accurate to better than 2% for $2 \leq \psi \leq 100$. Since $x_{\text{d}} = 1 - \tau_{\text{d}}/\tau_{\text{R}}$, this fixes x_{d} . Similarly, once τ_{d} is known it is straightforward to solve equation (37) to first order in τ_{R}^{-1} to obtain

$$x_{\text{H}_2} = 1 - \left[\tau_{\text{d}} + \frac{\psi}{2} E_3(\tau_{\text{d}}) \right] \tau_{\text{R}}^{-1}. \quad (56)$$

For $\psi < 2$, there is no dust-dominated zone, and we must instead solve equations (43) and (44) in the limit $\tau_{\text{R}} \rightarrow \infty$. We note that for a very large cloud $E^*(1) = E_0^*/2$ because the cloud blocks half the sky, and it therefore follows immediately from the definition of σ_{e} (equation 38) that

$$\tau_{\text{eR}} = \frac{2\tau_{\text{R}}}{\psi}, \quad (57)$$

i.e. that the effective molecular opacity is a factor of two larger than its free-space value because the radiation intensity at the cloud surface has half its free-space value. Similarly, the flux is $F^*(1) = F_0^*/4$ because half the sky is blocked and the radiation direction is random over the other half. Using this boundary condition to integrate the one-dimensional transfer-dissociation equation (10) with $\sigma_{\text{d}} = 0$ and the molecular absorption rate multiplied by ϕ then gives

$$x_{\text{H}_2} = 1 - \frac{\psi}{4\tau_{\text{R}}}. \quad (58)$$

We verify that these intuitive arguments in fact give the correct leading order terms in the series expansion in Appendix C. Thus we have the limiting solution to first order in τ_{R}^{-1} for both $\psi < 2$ and $\psi > 2$. We illustrate this solution for $\tau_{\text{R}} \rightarrow \infty$ in Figure 5.

4.5. Numerical Solution and Analytic Approximation

We now proceed with a numerical treatment of the general case. We solve equations (33) and (37), or (43) and (44), on a grid of points in the (τ_{R}, ψ) -plane, and plot the results in Figure 6. In addition to plotting x_{H_2} and either x_{d} or τ_{eR} , we also show two derived quantities of interest. The first is the dust optical depth to the molecular transition along a radial trajectory, $\tau_{\text{HI}} = nR(1 - x_{\text{H}_2})\sigma_{\text{d}}$. We may think of this as the HI “shielding column” times the dust cross section. The second is $x_{\text{H}_2}^3$, which is the fraction of the cloud’s volume that is within the predominantly molecular region.

The general behavior of these curves can be understood intuitively. If one fixes the cloud density n and dust opacity σ_{d} , then as the cloud radius increases so does τ_{R} , and for fixed external radiation field ψ the molecular transition moves outward, but the HI column to that transition approaches a constant value. Similarly, at fixed cloud size and hence τ_{R} , increasing the external illumination ψ raises the amount of atomic hydrogen that is required to shield the molecules. Thus x_{H_2} drops when ψ increases at fixed τ_{R} .

These curves also enable us to determine under what circumstances dust makes a significant contribution to shielding the gas, a subject that has been discussed considerably in the literature (e.g. van Dishoeck & Black 1986; Draine & Bertoldi 1996). To evaluate the importance of dust, we can consider how the molecular and atomic volumes change as $\sigma_{\text{d}} \rightarrow 0$. In terms of our parameters, this amounts to taking the limit as $\chi \rightarrow 0$ and $\tau_{\text{R}} \rightarrow 0$, but the ratio χ/τ_{R} remains constant. Graphically, this is equivalent to sliding toward the lower right of Figure 6, along a trajectory that is close to a line of slope unity – it is not precisely a line of slope unity because of the slight non-linearity of the relationship between ψ and χ . We plot the factor by which dust shielding changes the radius of the molecular zone or the radial path length through the atomic zone, whichever is larger, in Figure 7. As the figure shows, dust shielding changes the radius of the molecular zone by a factor of ~ 2 only when ψ is of order unity or larger or when τ_{R} is very large, which is about what one might expect. Dust shielding can affect the size of the molecular region even if there is no dust-dominated zone because we have allowed for dust absorptions even in the molecular shielding region. However, the effect is at most tens of percent. A larger change is possible only if the radiation field is intense enough to create a dust-dominated zone (i.e. $\psi \gtrsim 1$) or the cloud is so large (i.e. $\tau_{\text{R}} \gg 1$) that even weak dust shielding becomes significant because it attenuates the radiation exponentially rather than in a powerlaw fashion as do the molecules.

We can deduce approximate analytic fitting formulae for x_{H_2} by interpolating between the solutions for the limiting cases. The following fitting formulae are reasonably accurate and can be evaluated with no numerical

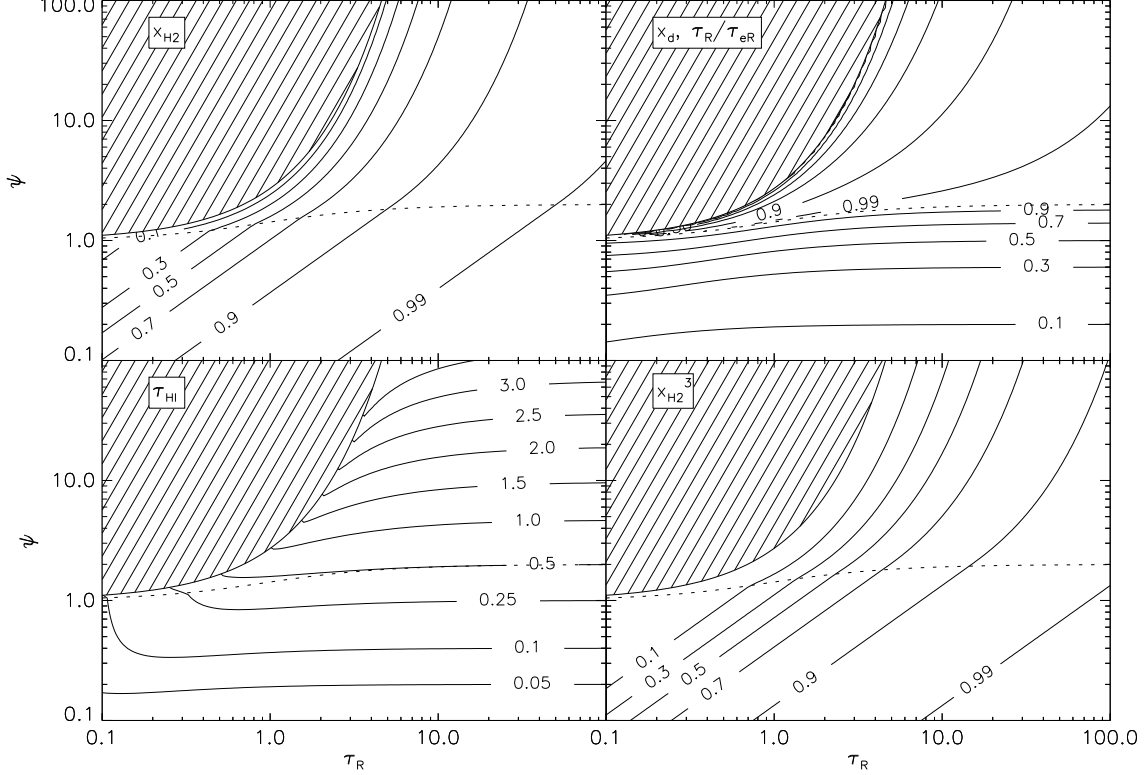


FIG. 6.— Contours showing the solution as a function of τ_R and ψ for the structure of the PDR in the two-zone approximation. The values shown are, clockwise from the upper left, x_{H_2} , x_d or τ_R/τ_{eR} , τ_{HI} , and $x_{\text{H}_2}^3$. The hatched region is the region in which there is no primarily molecular part of the cloud. The dotted line indicates the boundary between the presence and absence of a dust-dominated zone. In the panel labelled x_d , τ_R/τ_{eR} , the contours above the dotted line indicate the value of x_d , those below it show the value of τ_R/τ_{eR} , and on the dotted line both of these quantities are exactly 1.0. We caution that the contours for $x_{\text{H}_2} = 0.1$ and $x_{\text{H}_2} = 0.3$, and for $x_{\text{H}_2}^3 = 0.1$, should be regarded as giving upper limits on x_{H_2} , not precise estimates – see the discussion in § 4.7.

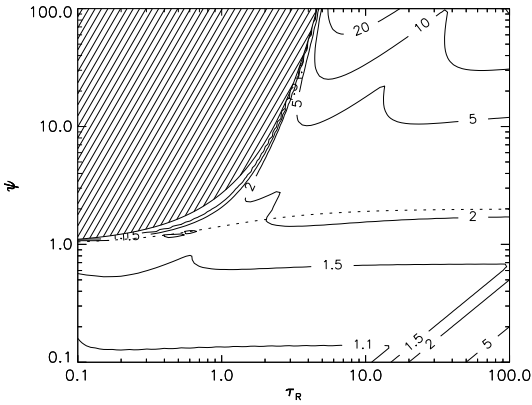


FIG. 7.— Contours showing the factor by which dust shielding changes the atomic or molecular volume at a given (τ_R, ψ) . The quantity plotted is $\max[x_{\text{H}_2}/x_{\text{H}_2,\text{nd}}, (1-x_{\text{H}_2,\text{nd}})/(1-x_{\text{H}_2})]$, where the subscript “nd” indicates the value with no dust shielding in the limit, i.e. in the limit $\sigma_d \rightarrow 0$. The quantity plotted is therefore the fractional amount by which dust shielding increases the radius of the molecular zone or decreases the radial path length through the atomic zone, whichever is larger.

iteration:

$$x_{\text{H}_2} \approx \begin{cases} \frac{\psi^4 x_s + (3\tau_R)^4 x_\ell}{\psi^4 + (3\tau_R)^4}, & \psi < 1 \\ \max(x_s, x_\ell), & 1 < \psi < \psi_b \\ \left(x_s^{-3/2} + x_\ell^{-3/2}\right)^{-2/3}, & \psi_b < \psi < 2 \\ \left(x_s^{-3} + x_\ell^{-3}\right)^{-1/3}, & 2 < \psi < e^{\tau_R} \\ 0, & e^{\tau_R} < \psi \end{cases} \quad (59)$$

where $\psi_b = (1.4 + 2\tau_R)/(1.4 + \tau_R)$ is the approximate value of ψ at the boundary between the existence and non-existence of a zone of dust-dominated opacity,

$$x_s^2 = \begin{cases} \left(\frac{\tau_R}{\sqrt{3}\psi} + \frac{2\sqrt{3}\tau_R^2}{5\psi^2}\right)^2, & \psi < 1 \\ 1 - \frac{1}{4\tau_b^2} \left[\ln\left(1 + 2\tau_b - 4\frac{\tau_b}{\psi}\right)\right]^2, & 1 < \psi < \psi_b \\ \left[\frac{1536}{25\tau_R(\tau_R+2)^3}\right]^{1/2} \left(\frac{e^{\tau_R}}{\psi} - 1\right)^{5/2}, & \psi_b < \psi \end{cases} \quad (60)$$

is the approximate value of x_{H_2} in the strong radiation (for $\psi > 1$) or small cloud (for $\psi < 1$) limits (note that

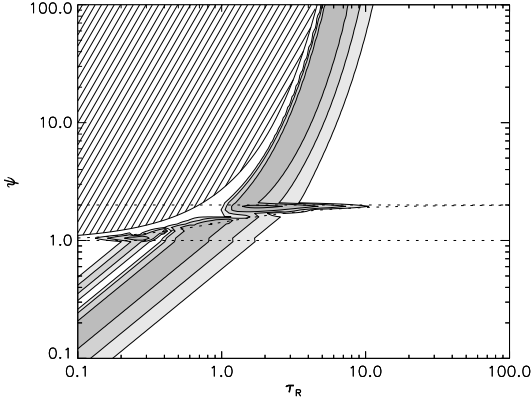


FIG. 8.— Error in the approximate analytic fit given in § 4.5 as a function of τ_R and ψ . The shaded regions indicate errors below 2.5% (*no shading*), 2.5–5%, 5–10%, 10–20%, and > 20% (*darkest shading*). The maximum error is 24%. The dotted lines show the boundaries of our different approximation regions: $\psi < 1$, $1 < \psi < \psi_b$, $\psi_b < \psi < 2$, and $2 < \psi$. The hatched region is $\psi > e^{\tau_R}$, where there is no predominantly molecular core. Note that the error jumps at the $\chi = 1$ and $\chi = 2$ lines because the fitting formula is slightly discontinuous there.

we only evaluate x_s when $\psi < e^{\tau_R}$, and

$$x_\ell^2 = \begin{cases} \left(\max \left[1 - \frac{\psi}{4\tau_R}, 0 \right] \right)^2, & \psi < \psi_b \\ 1 - \frac{1}{4\tau_b} \left[\ln \left(1 + 2\tau_b - 4\frac{\tau_b}{\psi} \right) \right]^2, & \psi_b < \psi < 2 \\ \left[1 - \left(\tau_d + \frac{\psi e^{-\tau_d}}{4+2\tau_d} \right) \frac{1}{\tau_R} \right]^2, & 2 < \psi \end{cases} \quad (61)$$

is the approximate value of x_{H_2} in the large cloud limit. Here

$$\tau_d = E_2^{-1} \left(\frac{2}{\psi} \right) \approx 0.83 \ln(0.2\psi + 0.6) \quad (62)$$

is the approximate optical depth to the dust-molecular opacity crossover in the large cloud limit when dust shielding is important,

$$\tau_b \approx 1.4 \frac{\psi - 1}{2 - \psi} \quad (63)$$

is the value of τ_R at the dust-no dust boundary for a given ψ , and for convenience we have used the approximation $E_3(x) \approx e^{-x}/(2+x)$. Note that these approximations can fail if one is very near the dust-no dust boundary because the approximation $\tau_b \approx 1.4(\psi-1)/(2-\psi)$ is insufficiently accurate; in this case one may still use the approximate expressions by replacing τ_b with a more accurate value of τ_R on the dust-no dust boundary computed as described in § 4.3.

Figure 8 shows the error in our analytic approximation as a function of τ_R and ψ , where we define the error as $|x_{\text{H}_2} - x_{\text{H}_2, \text{approx}}| / \max(x_{\text{H}_2}, 1 - x_{\text{H}_2})$ and x_{H_2} is the solution obtained by numerically solving the appropriate equations. As the plot shows the fitting formulae are generally good to the $\sim 10\%$ level, as good as the two-zone approximation itself. The maximum error over the range $0.1 < \tau_R < 100$ and $0.1 < \psi < 100$ is 24%, and occurs near $\tau_R = 1.8$, $\psi = 1.9$.

We can also obtain an even simpler approximation formula if we specialize to the case where there is no or almost no dust-dominated zone and $x_{\text{H}_2} \gtrsim 0.5$, which we

show in Paper II is the most common case in nearby galaxies. Consider equation (44), which describes the surface flux for the case of no dust. The two terms on the LHS represent the contributions to the flux from rays that do and do not pass through the cloud, respectively. If the cloud has a significant molecular core, $x_{\text{H}_2} \gtrsim 0.5$, then only for a small range of angles do rays pass through the cloud but not strike the opaque molecular core, and thus the first term on the LHS is small in comparison to the second. For convenience we define

$$\delta = \frac{1 - (1 - 2\mu_{\text{H}_2}\tau_{\text{eR}})e^{2\mu_{\text{H}_2}\tau_{\text{eR}}}}{2\tau_{\text{eR}}^2}, \quad (64)$$

which enables us to rewrite equation (44) as

$$x_{\text{H}_2}^3 = 1 - \frac{3\psi}{4\tau_R} (1 - \delta) \approx 1 - \frac{3\psi}{4\tau_R} \left(\frac{1}{1 + \delta} \right) \quad (65)$$

where δ is a small, positive number. Now consider how δ varies with τ_R : we show in § 4.4 that for either small or large τ_R , to first order $\tau_{\text{eR}} \propto \tau_R/\psi$. If we consider the series of expansion of δ , this implies that δ approaches a constant at small τ_R and varies as ψ^2/τ_R^2 for large τ_R . To generate our approximation we adopt an intermediate scaling

$$\delta \approx a \frac{\psi}{\tau_R}, \quad (66)$$

where a is a constant to be chosen to optimize the approximation. This gives

$$x_{\text{H}_2}^3 \approx 1 - \frac{3\psi}{4(\tau_R + a\psi)}. \quad (67)$$

For the choice $a = 0.2$, equation (67) agrees with the numerical solution to equations (33) and (37) or (43) and (44) to better than 15% whenever $\psi < 3$ and equation (67) gives $x_{\text{H}_2}^3 > 0.15$. A corresponding approximate formula for the optical depth through the atomic layer is

$$\tau_{\text{HI}} \approx \frac{\tau_R \psi}{4\tau_R - a'\psi}, \quad (68)$$

with $a' = \frac{3}{2} - 4a$. For $a = 0.2$ this expression agrees with the numerical solution to better than 15% for $\psi < 3$ whenever equation (67) gives $x_{\text{H}_2}^3 > 0.1$.

4.6. Comparison to the One-Dimensional Case

Now that we have solved the spherical case, we are in a position to compare to the case of a one-dimensional beam of radiation striking an infinite slab that is often treated in the literature. This will allow us to determine when this approximation yields reasonably accurate results, and when it is it gives significantly different results. Figure 9 shows a comparison between our solution with isotropic radiation and varying cloud sizes versus the most common approximation in the literature: an infinite cloud and a beam of radiation whose photon number density is half the free-space value. In the calculations for finite clouds and isotropic radiation we end each curve at the value of ψ for which the fully molecular region vanishes. For the beamed radiation and infinite cloud case, we use the analytic solution described in § 3.1.

As the plot shows, when $\tau_R \ll \psi$, the one-dimensional slab approximation can produce significantly different estimates of the depth of the dust shielding layer than does our higher-dimensional approach. The difference becomes larger as we consider smaller clouds. For $\tau_R > 1$ the slab approximation generally underestimates the depth of the atomic layer by tens of percent, primarily because it assumes neglects the photodissociation provided by non-radial rays. Even for a cloud that is infinitely large, $\tau_R = \infty$, this difference between an isotropic radiation field and a beamed one can be significant at moderate ψ because even though there are no rays reaching a given position from the “back side” of the cloud, $\mu < 0$, when the radiation field is isotropic there are still non-radial rays that raise the photodissociation rate at a given position above what it would be in the purely beamed radiation field of smaller intensity.

For $\tau_R < 1$ the sign of the error depends on ψ . When the radiation field is weak, the slab approximation also underestimates the depth of the atomic layer, for the same reason as when $\tau_R > 1$. When the radiation field becomes strong, though, the sign of the error reverses, although as we discuss in § 4.7 our fiducial model is of limited accuracy for small τ_R and large ψ .

Physically, clouds of a wide range of sizes and densities are of course present in the ISM. For the atomic envelopes of GMCs in the Milky Way, a typical density is $n \sim 30 \text{ cm}^{-3}$ and a typical dust cross-section is 10^{-21} cm^2 , so that $\sim 10 \text{ pc}$ of path provides an optical depth of about 1. Since these envelopes are a few tens of pc in size, a typical one might have τ_R of a few, in which case the slab treatment underestimates the true size of the envelope at the tens of percent level. In low-metallicity galaxies with low molecular fractions, however, the error is likely to be much worse because τ_R will be significantly smaller.

4.7. Uncertainties in Spherical Geometry

We have shown that in the case of a one-dimensional beam of radiation impinging on a slab, the two-zone approximation is capable of determining the neutral hydrogen shielding column to better than $\sim 50\%$ accuracy. This characterizes the level of error imposed by most of our physical assumptions. However, in spherical geometry we have an additional uncertainty, imposed by the fact that we must assign an effective optical depth to rays that pass at arbitrary angles through the region where molecular shielding dominates, but the gas is not yet fully molecular. In particular, rays from the “back side” of our cloud, those with $\mu < 0$, contribute to the energy density and flux throughout the cloud. Such rays are absent in the case of an infinite planar cloud, because rays with $\mu < 0$ pass through the fully molecular region and are therefore infinitely attenuated.

In this section, we seek to determine how much additional uncertainty is introduced into our calculations in spherical geometry by this complication. To do so, we note that in our treatment above we assume that the opacity in the molecular shielding region will be roughly equal to that at its surface, i.e. that it does not rise sharply until one is very close to the transition to fully molecular gas. This represents a minimum attenuation along $\mu < 0$ rays. To check the importance of that assumption, we consider an extreme assumption in the opposite direction: that all rays with $\mu < 0$ are infinitely

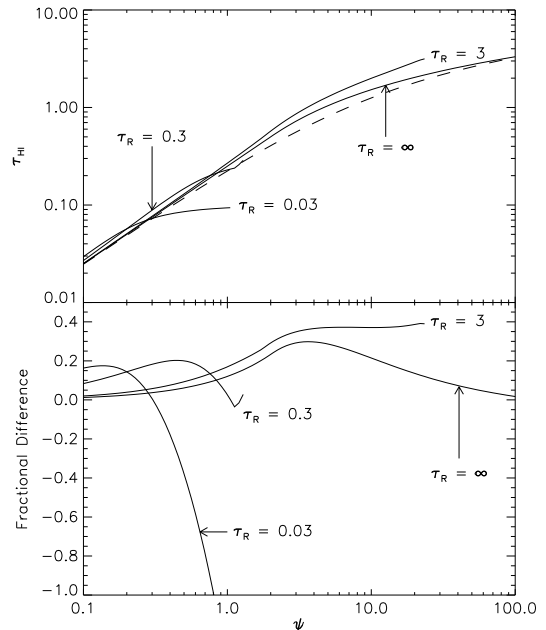


FIG. 9.— The upper panel shows the dust optical depth to the point where the gas becomes predominantly molecular τ_{HI} for an isotropic radiation field of normalized intensity ψ and various values of τ_R (solid lines) and for a unidirectional radiation field of normalized intensity $\psi/2$ (dashed line). The lower panel shows the fractional difference between the results for finite τ_R and isotropic radiation and for an infinite slab illuminated by unidirectional radiation, defined as $\text{Difference} = [\tau_{\text{HI,iso}} - \tau_{\text{HI,beam}}]/\tau_{\text{HI,iso}}$. In all cases the curves for finite τ_R end at the value of ψ for which fully molecular region disappears ($\psi = e^{\tau_R}$).

attenuated. This assumption is obviously unphysical, since if it were true then the transition to fully molecular would occur as soon as self-shielding began to dominate over dust shielding. However, it provides a worst case with which we can compare our fiducial model as a way of characterizing our uncertainty. Since, as we shall see, the value of x_{H_2} that we obtain by making this assumption is always smaller than what we obtain for the fiducial case, we may regard the fiducial case as giving upper limit on x_{H_2} and the case we calculate here as giving a lower limit.

If we take the intensity along rays with $\mu < 0$ to be zero, this is equivalent to replacing $\eta_0(x_d, x_{\text{H}_2}; \tau_R)$ with $\eta_0(x_d, x_d; \tau_R)$ in the equations derived in § 4.1 and § 4.2, and similarly for η_1 . Doing this and simplifying gives

$$\eta_0(x_d, x_d; \tau_R) = \frac{1}{\psi} \quad (69)$$

$$\eta_1(x_d, x_d; \tau_R) = \frac{\tau_R x_d}{3\psi} \left[1 - \left(\frac{x_{\text{H}_2}}{x_d} \right)^3 \right] \quad (70)$$

for $\psi > 2$ (dust shielding is significant) and

$$x_{\text{H}_2} = \left(1 - \frac{3\psi}{4\tau_R} \right)^{1/3} \quad (71)$$

for $\psi < 2$ (dust shielding is not significant). Note that in this case when dust shielding is negligible it is possible to solve the equations analytically, which we have done to obtain equation (71). It is immediately obvious from this

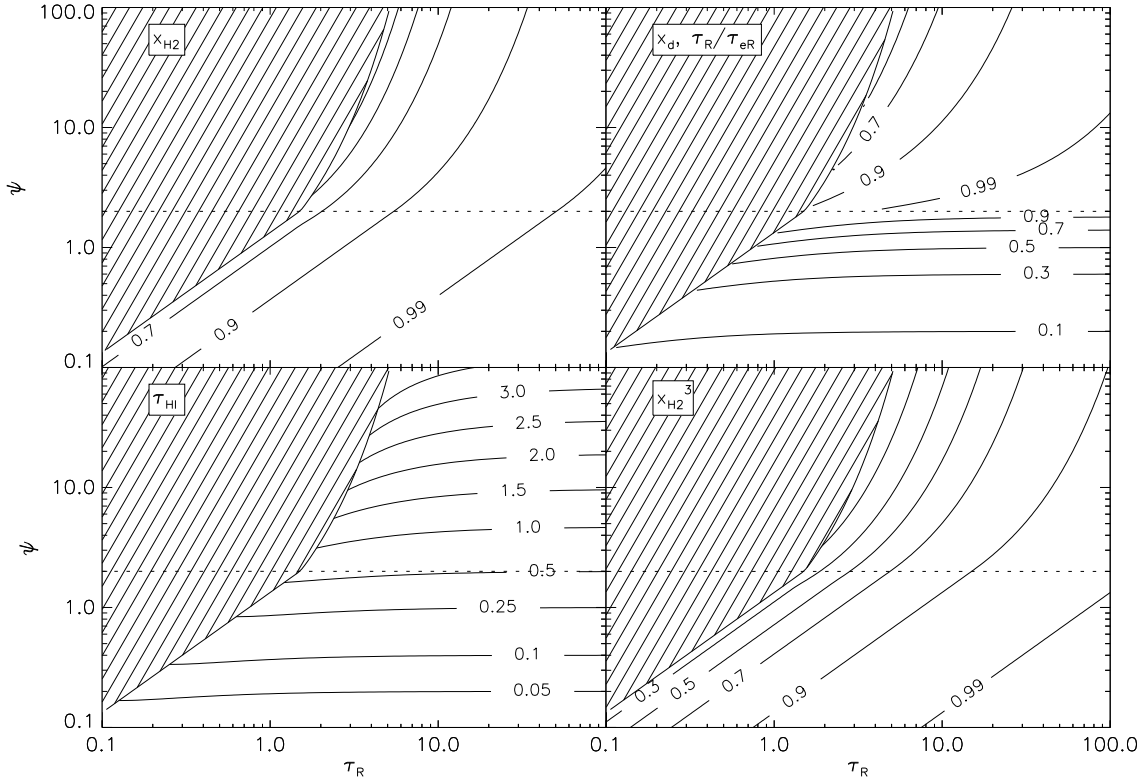


FIG. 10.— Same as Figure 6, but assuming infinite attenuation along rays that enter the molecular absorption-dominated region (equations 69–71).

equation that the fully molecular region vanishes in the region $4\tau_R/3 < \psi < 2$. We plot the solutions to equations (69)–(71) in the (τ_R, ψ) plane in Figure 10, and we show the difference between this solution and our fiducial one in Figure 11.

As the plots show, the difference between the two models is negligibly small over most of parameter space; there is a significant difference only in the region roughly bounded by the curves $\psi \lesssim e^{\tau_R}$, $\psi \gtrsim 4\tau_R/3$, and $\psi \lesssim 2$. Alternately, we can phrase these constraints in terms of values of $x_{\text{H}_2}^3$. This is particularly useful for $\psi < 1$, where contours of both constant x_{H_2} and constant uncertainty are both straight lines corresponding to fixed ψ/τ_R . The 10%, 50%, and 100% uncertainty contours in $x_{\text{H}_2}^3$, shown in the right panel of Figure 11, correspond to values of $x_{\text{H}_2}^3 = 0.47, 0.28,$ and 0.20 , respectively, as computed using our fiducial model and shown in Figure 11. Since we have already established that the two-zone approximation is uncertain at the tens of percent level, the geometric uncertainty is probably only dominant when $\psi < 1$ and our predicted molecular volume fraction $x_{\text{H}_2}^3$ is less than about a quarter. If $\psi \gtrsim 1$, the errors at a given value of $x_{\text{H}_2}^3$ are considerably smaller, so the geometric uncertainty is not important except for clouds with very small molecular fractions. At such molecular fractions, one should interpret our fiducial case as giving only an upper limit on the molecular content of a cloud.

The significant geometric uncertainty for such clouds is not surprising, since these clouds are near the limit of having no molecules at all. For them any change in our physical assumptions that increases or reduces the

amount of shielding even a small amount produces a significant change in the results. Indeed, our fiducial calculation shows some unphysical behavior in this regime, in that we find that for $\psi < 1$ there is no finite value of τ_R for which the fully molecular region vanishes and the cloud remains atomic throughout. This seems unlikely, given that for a chosen value of ψ and very large τ_R the thickness of the atomic region approaches a finite value; one would expect that clouds much smaller than this should be atomic throughout regardless of their shape, and indeed under the assumption of infinite attenuation for backside rays that we make in this section, the molecular core always vanishes at some finite value of τ_R for any finite ψ .

Fortunately, as we discuss in § 4.8, for realistic parameters describing giant atomic-molecular complexes, we generally have $\psi \gtrsim 1$, $\tau_R \gtrsim 1$, and, as we show in § 4.8, $x_{\text{H}_2}^3 \gtrsim 0.5$, and in this part of parameter space the uncertainty introduced by the $\mu < 0$ rays in spherical geometry is $\lesssim 10\%$.

4.8. Example Calculations

Here we provide examples that illustrate the use of our analytic approximations for PDR structure. Since these calculations are intended to be illustrative rather than to analyze real situations (which we will discuss in the next paper in this series), we choose parameters to yield examples that span the possible combinations of parameters without worrying how well they agree with observations. As a first case, consider a “typical” Milky Way cloud, with $\sigma_d = 1.1 \times 10^{-21} \text{ cm}^2$, $n = 30 \text{ cm}^{-3}$,

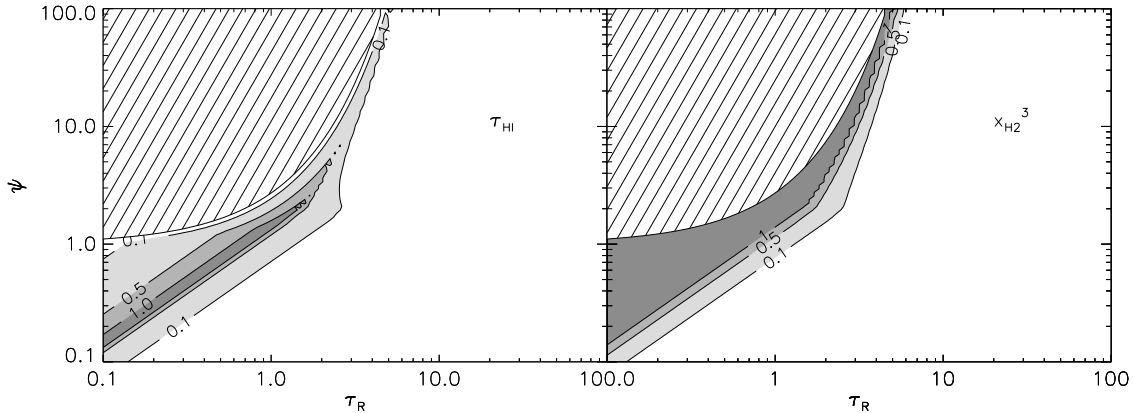


FIG. 11.— The plots show the difference between τ_{HI} and $x_{\text{H}_2}^3$ computed under the fiducial assumption that the opacity throughout the molecule-dominated region equal to that at its surface (§ 4.1 and § 4.2) and under the assumption of infinite attenuation in this region (§ 4.7). The difference is defined as $|\tau_{\text{HI, fiducial}} - \tau_{\text{HI, attenuated}}|/\tau_{\text{HI, fiducial}}$, and similarly for $x_{\text{H}_2}^3$. The hatched region is the region in which there is no predominantly molecular core under either assumption; the difference in this region is obviously zero.

$\mathcal{R} = 3 \times 10^{-17} \text{ cm}^3 \text{ s}^{-1}$, and $cE_0^* = 10^8 \text{ cm}^{-2} \text{ s}^{-1}$. Note that we have used a value of E_0^* somewhat larger than the solar neighborhood value because most molecular clouds are closer to the galactic center, where the radiation field is more intense. This combination of parameters gives $\chi = f_{\text{diss}} \sigma_{\text{d}} cE_0^* / (n\mathcal{R}) = 12.2$ and $\psi = \chi(2.5 + \chi)/(2.5 + \chi e) = 6.3$. Now consider a giant molecular cloud complex with a radius $R = 50 \text{ pc}$, which gives $\tau_{\text{R}} = n\sigma_{\text{d}}R = 4.64$. Since $\psi > 2$, this cloud has a significant dust shielding zone, and since $\psi < e^{\tau_{\text{R}}}$ it also has a fully molecular core, as we expect. Using the approximation equations (59)–(61) for this case, we find $\tau_{\text{d}} = 0.52$, $x_{\ell} = 0.74$, $x_{\text{s}} = 14.1$, and an approximate value of $x_{\text{H}_2} \approx 0.74$. (Note that although x_{H_2} is strictly less than unity, it is possible for x_{s} to be larger than unity because we only retained a finite number of terms in the series expansion used to generate it. However, due to the way x_{s} and x_{ℓ} are combined, our approximate expression for x_{H_2} is always less than unity.) Numerical solution for these parameters gives $x_{\text{H}_2} = 0.70$. Such a cloud is 34% molecular by volume, and is shielded by an atomic column that is 15 pc deep and has a column density of $N_{\text{HI}} = 1.4 \times 10^{21} \text{ cm}^{-2}$ from the edge the cloud to the edge of the molecular zone.

Now consider moving this cloud to a point farther out in the Galaxy where the ambient FUV radiation field is weaker, so that all cloud parameters remain the same but now $cE_0^* = 2 \times 10^7 \text{ cm}^{-2} \text{ s}^{-1}$, a factor of 5 below our previous value. In this case we have the same τ_{R} , but $\chi = 2.44$ and $\psi = 1.43$. For this τ_{R} we have $\psi_{\text{b}} = 1.40$, slightly smaller than ψ , so this cloud just barely still has a dust-dominated zone. Evaluating equations (59)–(61), we have $x_{\ell} = 0.87$ and $x_{\text{s}} = 95$, so get an approximate value $x_{\text{H}_2} \approx 0.87$; the numerical solution is $x_{\text{H}_2} = 0.92$. Thus moving the cloud to this reduced-radiation environment raises the molecular volume fraction to 77%, and reduces the HI shielding column to a layer 4 pc deep containing a column of $N_{\text{HI}} = 3.7 \times 10^{20} \text{ cm}^{-2}$ hydrogen atoms. If the cloud were slightly denser, $n = 40 \text{ cm}^{-3}$ instead of 30 cm^{-3} , then τ_{R} would increase to 6.18 from 4.64, and ψ would decrease to 1.11 from 1.43. Since $\psi_{\text{b}} = 1.82$ in this case, the cloud would be dominated by molecular absorption throughout. Evaluating the ap-

proximation equations gives $x_{\ell} = 0.95$, $x_{\text{s}} = 0.35$, and $x_{\text{H}_2} \approx 0.95$; the numerical solution is $x_{\text{H}_2} = 0.95$. Thus, the increase in density would slightly increase the molecular volume and the column density through the shielding layer to 87% and $N_{\text{HI}} = 5.2 \times 10^{20} \text{ cm}^{-2}$, respectively.

Finally consider a cloud in a low-pressure dwarf galaxy with a very low star formation rate, so the cloud has lower density and metallicity than a Milky Way cloud, $n = 10 \text{ cm}^{-3}$, $\sigma_{\text{d}} = 2.2 \times 10^{-22}$, and $\mathcal{R} = 6 \times 10^{-18}$, and is exposed to a lower level of radiation, $cE_0^* = 10^6 \text{ cm}^{-2} \text{ s}^{-1}$. We keep the cloud radius unchanged. This cloud has $\tau_{\text{R}} = 0.31$ and $\psi = 0.29$, which from our approximate formulae gives $x_{\ell} = 0.77$, $x_{\text{s}} = 1.4$, and $x_{\text{H}_2} \approx 0.77$. The numerical solution is $x_{\text{H}_2} = 0.73$. This cloud would be 38% molecular by volume, and would have a shielding layer of $N_{\text{HI}} = 4.2 \times 10^{20} \text{ cm}^{-2}$, 14 pc deep.

5. SUMMARY AND CONCLUSION

In this paper we develop an approximate analytic solution to the problem of determining the size of the PDR that bounds a cloud of gas embedded in a dissociating background radiation field. This is a reasonable approximation to the problem of finding the location of the transition between the atomic envelope and the molecular core in a giant atomic-molecular cloud complex, such as those which contain the bulk of the molecular gas in the Milky Way.

We show that the location of the transition is determined by two dimensionless parameters. These are τ_{R} , the dust optical depth through the cloud, and χ , the ratio of the rate at which dissociating photons are absorbed by dust grains to the rate at which they are absorbed by H_2 molecules in the absence of any shielding. We may intuitively think of these parameters as characterizing the size of the cloud and the intensity of the radiation field to which it is subjected. Within this parameter space we identify two critical curves, which define the boundaries at which a fully molecular region in the cloud center appears, and at which dust shielding begins to contribute significantly to the shielding of H_2 molecules. We develop the equations that determine the sizes of the molecular and atomic regions in this parameter space, and we provide an approximate analytic solution for them (equa-

tions 59 – 61 and equations 67 and 68). Our solutions are accurate to tens of percent for clouds that are $\gtrsim 20\%$ molecular by volume, and provide upper limits on the molecular content at this accuracy for clouds with lower molecular content. Using this formalism we find that for typical giant atomic-molecular complexes in the Milky Way $\chi \sim 1$, which indicates that dust shielding and self-shielding each make order unity contributions to determining the location of the atomic-molecular transition.

Our work shows that the procedure of determining the structure of PDRs by treating them as semi-infinite slabs illuminated by unidirectional beams of dissociating radiation is a reasonable approximation for extremely opaque clouds, but that it fails badly for small clouds or weak radiation fields, i.e. in cases where the transition from atomic to molecular is sufficiently far into the cloud that the cloud's curvature cannot reasonably be neglected. In such cases the slab approximation can either overestimate or underestimate the size of the atomic layer by factors of order unity, depending on the particular parameters of the cloud and the ambient radiation field.

The development of an analytic model for the structure of the atomic envelopes of finite molecular clouds opens up the possibility of developing a more general theory of the atomic to molecular ratio in galaxies. In a galaxy, the mean interstellar radiation field and the conditions in the atomic portion of the atomic interstellar medium are determined by the star formation rate, which determines the abundance of young, hot stars. In turn, the star for-

mation rate depends on the fraction of the ISM of that galaxy in molecular form, and therefore available for star formation. At some level, therefore, star formation in galaxies must be a self-regulating process, with the formation and dissociation of molecular clouds representing one step in that regulation. Developing a simple model for how the molecular fraction in a cloud is determined by its properties and those of the ambient radiation field represents a step toward a complete theory of the star formation rate. In future work, we plan to develop this theory further by applying the model demonstrated here to molecular clouds in galaxies.

We thank B. Draine and J. Goodman for helpful discussions, and the anonymous referee for useful comments. Support for this work was provided by NASA through Hubble Fellowship grant #HSF-HF-01186 awarded by the Space Telescope Science Institute, which is operated by the Association of Universities for Research in Astronomy, Inc., for NASA, under contract NAS 5-26555 (MRK), and by the National Science Foundation through grants AST-0098365 (to CFM) and PHY05-51164 (to the Kavli Institute for Theoretical Physics, where MRK, CFM, and JT collaborated on this work). JT gratefully acknowledges the support of Gilbert and Jaylee Mead for their namesake fellowship in the Yale Center for Astronomy and Astrophysics.

APPENDIX

A. EVALUATION OF η_0 AND η_1

Here we evaluate the two functions

$$\eta_0(x_d, x_{H_2}; \tau_R) = \frac{1}{2} \int_{\mu_{H_2}}^1 d\mu \exp(-\tau_R \xi) \quad (A1)$$

$$\eta_1(x_d, x_{H_2}; \tau_R) = \frac{1}{2} \int_{\mu_{H_2}}^1 d\mu \mu \exp(-\tau_R \xi). \quad (A2)$$

To evaluate the integrals, we change the variable of integration from μ to ξ . Using the definition of ξ (equation 29), we find that

$$\mu = \frac{(1 - x_d)(1 + x_d) - \xi^2}{2x_d \xi} \quad (A3)$$

and

$$\frac{d\mu}{d\xi} = -\frac{(1 - x_d)(1 + x_d) + \xi^2}{2x_d \xi^2}. \quad (A4)$$

Making the change of variable, we find that

$$\eta_0(x_d, x_{H_2}; \tau_R) = -\frac{1}{4x_d} \left[\int_{\xi_{H_2}}^{1-x_d} d\xi \exp(-\xi \tau_R) + (1 - x_d)(1 + x_d) \int_{\xi_{H_2}}^{1-x_d} d\xi \xi^{-2} \exp(-\xi \tau_R) \right] \quad (A5)$$

$$\eta_1(x_d, x_{H_2}; \tau_R) = \frac{1}{8x_d^2} \left[\int_{\xi_{H_2}}^{1-x_d} d\xi \xi \exp(-\xi \tau_R) - (1 - x_d)^2 (1 + x_d)^2 \int_{\xi_{H_2}}^{1-x_d} d\xi \xi^{-3} \exp(-\xi \tau_R) \right], \quad (A6)$$

where

$$\xi_{H_2} \equiv \xi(x_d, \mu_{H_2}) = \sqrt{1 - x_d^2 + x_d^2 \mu_{H_2}^2} - x_d \mu_{H_2}. \quad (A7)$$

Of these integrals, the first one for η_0 may be evaluated directly, while the first one for η_1 may be evaluated by parts. The second integral on each line may be evaluated via the identity

$$\int_{x_0}^{x_1} dx x^{-n} e^{-ax} = \int_{x_0}^{\infty} dx x^{-n} e^{-ax} - \int_{x_1}^{\infty} dx x^{-n} e^{-ax} \quad (\text{A8})$$

$$= x_0^{1-n} \int_1^{\infty} du u^{-n} e^{-ax_0 u} - x_1^{1-n} \int_1^{\infty} dv v^{-n} e^{-ax_1 v} \quad (\text{A9})$$

$$= x_0^{1-n} E_n(ax_0) - x_1^{1-n} E_n(ax_1), \quad (\text{A10})$$

where in the second step we made the change of variables $u = x/x_0$ and $v = x/x_1$, and E_n is the exponential integral function of order n , defined by $E_n(x) = \int_1^{\infty} t^{-n} e^{-xt} dt$. Using this identity gives

$$\eta_0(x_d, x_{H_2}; \tau_R) = \frac{1}{4x_d} \left\{ \frac{e^{-y_d \tau_R} - e^{-\xi_{H_2} \tau_R}}{\tau_R} + (1 + x_d) \left[E_2(y_d \tau_R) - \frac{y_d}{\xi_{H_2}} E_2(\xi_{H_2} \tau_R) \right] \right\} \quad (\text{A11})$$

$$\eta_1(x_d, x_{H_2}; \tau_R) = \frac{1}{8x_d^2} \left\{ \frac{(1 + \xi_{H_2} \tau_R) e^{-\xi_{H_2} \tau_R} - (1 + y_d \tau_R) e^{-y_d \tau_R}}{\tau_R^2} + (1 + x_d)^2 \left[E_3(y_d \tau_R) - \frac{y_d^2}{\xi_{H_2}^2} E_3(\xi_{H_2} \tau_R) \right] \right\}, \quad (\text{A12})$$

where $y_d \equiv 1 - x_d$. Note that exponential integrals obey the recurrence relation $n E_{n+1}(x) = e^{-x} - x E_n(x)$, so we could alternately have written these in terms of $E_1(x)$ or the classical exponential integral $\text{Ei}(x) = -E_1(-x)$.

B. SOLUTION BY SERIES EXPANSION IN THE STRONG RADIATION LIMIT

Here we solve equations (33) and (37) in the strong radiation limit, i.e. $x_{H_2} \ll 1$, $x_d \ll 1$, and $\mu_{H_2} + 1 \ll 1$, by means of series expansion. Let $\beta = x_d \tau_R$ and $\gamma = 1 + \mu_{H_2}$. Then we have

$$e^{-\tau_R \xi} = e^{-\tau_R} \left[1 + \mu \beta + \left(\frac{1}{2\tau_R} + \frac{\tau_R + 1}{2\tau_R} \mu^2 \right) \beta^2 + \left(\frac{1}{2\tau_R} \mu + \frac{\tau_R - 3}{6\tau_R} \mu^3 \right) \beta^3 + O(\beta^4) \right]. \quad (\text{B1})$$

Note that we have retained terms out to order β^3 . We shall see below that this is required for a consistent solution. Using this expansion in the integrals

$$\eta_0(x_d, x_{H_2}; \tau_R) = \frac{1}{2} \int_{\gamma-1}^1 d\mu e^{-\tau_R \xi} \quad (\text{B2})$$

$$\eta_1(x_d, x_{H_2}; \tau_R) = \frac{1}{2} \int_{\gamma-1}^1 d\mu \mu e^{\tau_R \xi} \quad (\text{B3})$$

and expanding in powers of γ , we find

$$\eta_0(x_d, x_{H_2}; \tau_R) = \frac{e^{-\tau_R}}{2} \left[2 - \gamma + \gamma \beta + \frac{\tau_R + 2}{3\tau_R} \beta^2 + O(\beta^4) + O(\gamma \beta^2) + O(\gamma^2) \right] \quad (\text{B4})$$

$$\eta_1(x_d, x_{H_2}; \tau_R) = \frac{e^{-\tau_R}}{2} \left[\frac{2}{3} \beta + \gamma - \gamma \beta + \frac{\tau_R + 2}{15} \beta^3 + O(\beta^4) + O(\gamma \beta^2) + O(\gamma^2) \right]. \quad (\text{B5})$$

If we similarly expand the right-hand sides of (33) and (37) in powers of β and γ , we obtain the two equations

$$\frac{e^{-\tau_R}}{2} \left[2 - \gamma + \gamma \beta + \frac{\tau_R + 2}{3\tau_R} \beta^2 \right] = \frac{1}{\psi} + O(\beta^4) + O(\gamma \beta^2) + O(\gamma^2) \quad (\text{B6})$$

$$\frac{e^{-\tau_R}}{2} \left[\frac{2}{3} \beta + \gamma - \gamma \beta + \frac{\tau_R + 2}{15} \beta^3 \right] = \frac{\beta}{3\psi} + O(\beta^4) + O(\gamma \beta^2) + O(\gamma^2). \quad (\text{B7})$$

If we combine these two equations by eliminating the common factor $e^{\tau_R/\psi}$, we obtain an equation for the relationship between β and γ :

$$-\frac{\gamma}{2} + \frac{\gamma \beta}{2} + \frac{\tau_R + 2}{6\tau_R} \beta^2 = \frac{3}{2} \left(\frac{\gamma}{\beta} \right) - \frac{3}{2} \gamma + \frac{\tau_R + 2}{10\tau_R} \beta^2 + O(\beta^3) + O(\gamma \beta) + O\left(\frac{\gamma^2}{\beta} \right). \quad (\text{B8})$$

The only way for this equation to have a consistent solution in which the orders on both sides balance is if γ is of order β^3 . In this case the leading order on both sides is β^2 (an order we retained only by performing the expansion in equation B1 to order β^3), and balancing the leading order terms gives

$$\gamma = \frac{2\tau_R + 4}{45\tau_R} \beta^3. \quad (\text{B9})$$

Since we now know the order of all terms, we can solve equation (B6) to leading order to obtain

$$x_d = \frac{\beta}{\tau_R} = \left[\frac{6}{\tau_R(\tau_R + 2)} \left(\frac{e^{\tau_R}}{\psi} - 1 \right) \right]^{1/2}. \quad (\text{B10})$$

Similarly, we know that

$$\left(\frac{x_{\text{H}_2}}{x_d} \right)^2 = 1 - \mu_{\text{H}_2}^2 = 2\gamma + O(\gamma^2). \quad (\text{B11})$$

Substituting (B9) for γ and (B10) for x_d and re-arranging, we obtain to leading order

$$x_{\text{H}_2} = \left[\frac{1536}{25\tau_R(\tau_R + 2)^3} \right]^{1/4} \left(\frac{e^{\tau_R}}{\psi} - 1 \right)^{5/4}. \quad (\text{B12})$$

C. SOLUTION BY SERIES EXPANSION IN THE LARGE AND SMALL CLOUD LIMITS

Here we solve equations (43) and (44) by series expansion in the limits $\tau_R \rightarrow 0$ and $\tau_R \rightarrow \infty$. We approach this problem by defining $\beta = \tau_{\text{eR}}/\tau_R$, so that with some rearrangement the equations are

$$1 - e^{2\beta\mu_{\text{H}_2}\tau_R} + 2\beta\tau_R - \frac{4}{\psi}\tau_R = 0 \quad (\text{C1})$$

$$(1 - 2\beta\mu_{\text{H}_2}\tau_R)e^{2\beta\mu_{\text{H}_2}\tau_R} - 1 + 2\beta^2\tau_R^2 - \frac{8}{3\psi}\beta^2\tau_R^3 \left[1 - (1 - \mu_{\text{H}_2}^2)^{3/2} \right] = 0. \quad (\text{C2})$$

For the case $\tau_R \rightarrow 0$ we then let

$$\beta = \beta_0 + \beta_1\tau_R + \beta_2\tau_R^2 + \dots \quad (\text{C3})$$

$$\mu_{\text{H}_2} = \mu_0 + \mu_1\tau_R + \mu_2\tau_R^2 + \dots \quad (\text{C4})$$

Expanding equations (C1) and (C2) to leading order in τ_R and re-arranging gives

$$2\beta_0(1 - \mu_0) - \frac{4}{\psi} = 0 \quad (\text{C5})$$

$$2\beta_0^2(1 - \mu_0^2) = 0, \quad (\text{C6})$$

which has the solution $\mu_0 = -1$, $\beta_0 = 1/\psi$. Using these values and continuing the expansion to the next order, we obtain

$$-2\beta_1 + \frac{1 + \mu_1\psi}{\psi^2} = 0 \quad (\text{C7})$$

$$\frac{4\mu_1}{\psi^2} = 0, \quad (\text{C8})$$

so $\mu_1 = 0$ and $\beta_1 = 1/(2\psi^2)$. Continuing to one more order, we have

$$4\beta_2 - \frac{2 + 6\beta_2\psi^2}{3\psi^3} = 0 \quad (\text{C9})$$

$$-1 + 6\mu_2\psi^2 = 0, \quad (\text{C10})$$

so $\mu_2 = 1/(6\psi^2)$ and $\beta_2 = 1/(4\psi^3)$. It improves the accuracy of the approximation for x_{H_2} significantly at small ψ to include one more order, so we do so:

$$4\beta_3 + \frac{1}{3\psi^4} - \frac{2}{\psi}\mu_3 = 0 \quad (\text{C11})$$

$$\frac{4}{\psi^2}\mu_3 - \frac{8}{5\psi^5} = 0, \quad (\text{C12})$$

so $\mu_3 = 2/(5\psi^3)$ and $\beta_3 = 7/(60\psi^4)$. Therefore to order τ_R^4 we have

$$\frac{\tau_{\text{eR}}}{\tau_R} = \frac{1}{\psi} + \frac{\tau_R}{2\psi^2} + \frac{\tau_R^2}{4\psi^3} + \frac{7\tau_R^3}{60\psi^4} \quad (\text{C13})$$

$$\mu_{\text{H}_2} = -1 + \frac{\tau_R^2}{6\psi^2} + \frac{2\tau_R^3}{5\psi^3} \quad (\text{C14})$$

$$x_{\text{H}_2} = \sqrt{1 - \mu_{\text{H}_2}^2} = \frac{\tau_R}{\sqrt{3}\psi} + \frac{2\sqrt{3}\tau_R^2}{5\psi^2}. \quad (\text{C15})$$

For the case $\tau_R \rightarrow \infty$, we let

$$\beta = \beta_0 + \beta_{-1/2}\tau_R^{-1/2} + \beta_{-1}\tau_R^{-1} + \dots \quad (\text{C16})$$

$$\mu_{\text{H}_2} = \mu_0 + \mu_{-1/2}\tau_R^{-1/2} + \mu_{-1}\tau_R^{-1} + \dots, \quad (\text{C17})$$

and if we expand equations (C1) and (C2) in powers of τ_R^{-1} then the leading order equations are

$$2\beta_0 - \frac{4}{\psi} = 0 \quad (\text{C18})$$

$$-\frac{8}{3\psi} \left[1 - (1 - \mu_0^2)^{3/2} \right] = 0. \quad (\text{C19})$$

Therefore $\beta_0 = 2/\psi$ and $\mu_0 = 0$. Continuing the expansion to the next order,

$$2\beta_{-1/2} = 0 \quad (\text{C20})$$

$$-\frac{16}{\psi^3}\mu_{-1/2}^2 + \frac{8}{\psi^2} = 0, \quad (\text{C21})$$

so $\beta_{-1/2} = 0$ and $\mu_{-1/2} = -\sqrt{\psi/2}$. Continuing one more order,

$$1 + 2\beta_{-1} = 0 \quad (\text{C22})$$

$$\frac{16\sqrt{2}}{\psi^5/2}\mu_{-1} = 0, \quad (\text{C23})$$

so $\beta_{-1} = -1/2$ and $\mu_{-1} = 0$. Thus to order τ_R^{-1} in the limit $\tau_R \rightarrow \infty$ we have

$$\frac{\tau_{\text{eR}}}{\tau_R} = \frac{2}{\psi} \quad (\text{C24})$$

$$\mu_{\text{H}_2} = -\sqrt{\frac{\psi}{2\tau_R}} \quad (\text{C25})$$

$$x_{\text{H}_2} = 1 - \frac{\psi}{4\tau_R}. \quad (\text{C26})$$

REFERENCES

- Allen, R. J., Heaton, H. I., & Kaufman, M. J. 2004, *ApJ*, 608, 314
 Black, J. H. & van Dishoeck, E. F. 1987, *ApJ*, 322, 412
 Blitz, L. & Rosolowsky, E. 2006, *ApJ*, 650, 933
 Browning, M. K., Tumlinson, J., & Shull, J. M. 2003, *ApJ*, 582, 810
 Cardelli, J. A., Clayton, G. C., & Mathis, J. S. 1989, *ApJ*, 345, 245
 Draine, B. T. 1978, *ApJS*, 36, 595
 Draine, B. T. & Bertoldi, F. 1996, *ApJ*, 468, 269
 Elmegreen, B. G. 1993, *ApJ*, 411, 170
 Elmegreen, B. G. & Elmegreen, D. M. 1987, *ApJ*, 320, 182
 Federman, S. R., Glassgold, A. E., & Kwan, J. 1979, *ApJ*, 227, 466
 Hollenbach, D. J. & Tielens, A. G. G. M. 1999, *Reviews of Modern Physics*, 71, 173
 Liszt, H. 2002, *A&A*, 389, 393
 Liszt, H. & Lucas, R. 2000, *A&A*, 355, 333
 Neufeld, D. A. & Spaans, M. 1996, *ApJ*, 473, 894
 Roberge, W. G., Dalgarno, A., & Flannery, B. P. 1981, *ApJ*, 243, 817
 Spaans, M. & Neufeld, D. A. 1997, *ApJ*, 484, 785
 Sternberg, A. 1988, *ApJ*, 332, 400
 van Dishoeck, E. F. & Black, J. H. 1986, *ApJS*, 62, 109
 Wolfire, M. G., Tielens, A. G. G. M., Hollenbach, D., & Kaufman, M. J. 2008, *ApJ*